

A peculiar low-luminosity short gamma-ray burst from a double neutron star merger progenitor

B.-B. Zhang^{1,2}, B. Zhang^{3,4,5}, H. Sun⁶, W.-H. Lei⁷, H. Gao⁸, Y. Li⁵, L. Shao^{9,10}, Y. Zhao¹¹, Y.-D. Hu^{1,12}, H.-J. Lü¹³, X.-F. Wu^{10,14}, X.-L. Fan¹⁵, G. Wang^{16,17}, A. J. Castro-Tirado^{1,18}, S. Zhang⁹, B.-Y. Yu⁹, Y.-Y. Cao⁹, E.-W. Liang¹³

Short-duration gamma-ray bursts (sGRBs) have long been proposed to be produced in systems involving the coalescence of double neutron stars (NS-NS) [1], and the observations of sGRB afterglows and host galaxies are consistent with such a conjecture [2–4]. Based on the estimated event rate density derived from previously observed sGRBs at cosmological distances [5, 6], the chance of detecting a sGRB within a small volume for detectable NS-NS mergers by advanced LIGO is very low [7]. On August 17, 2017, coinciding with a double neutron star merger gravitational wave event detected by the LIGO-Virgo gravitational wave detector network [8], a short-duration GRB 170817A was detected by both Gamma-Ray Monitor (GBM) on board NASA’s Fermi Gamma-Ray Observatory [9] and INTEGRAL [10]. Here we show that the fluence ($\sim 4.46 \times 10^{-7}$ erg cm⁻²) and spectral peak energy (~ 158 keV) of this sGRB fall into the lower portion of the distributions of known sGRBs. With a very small distance from Earth [11], its peak isotropic luminosity ($\sim 1.7 \times 10^{47}$ erg s⁻¹) is abnormally low. With its detection, the estimated event rate density above this luminosity is at least 190^{+440}_{-160} Gpc⁻³ yr⁻¹, which is close to but still below the NS-NS merger event rate density. The low-luminosity sGRB may originate from a structured jet viewed from a large viewing angle. Alternatively, not all NS-NS mergers produce energetic jets. There are similar faint soft GRBs in the Fermi GBM archival data, a small fraction of which might belong to this new population of nearby, low-luminosity sGRBs.

GRB 170817A (*Fermi* Trigger number 170817529) triggered Fermi GBM (8 keV - 40 MeV) [12] at $T_0=12:41:06.474598$ UT on 17 August 2017 [9]. We process the public Fermi/GBM data using the standard software package [13]. We selected two GBM/NaI detectors, n1 and n2, on board *Fermi* that are in good geometric configurations (e.g., angle < 60 deg) with respect to the source position. By extracting the photon events from the un-binned Time-Tagged Event (TTE) data detected by these two detectors, we noticed that a sharp peak is presented in the light curve between $T_0 - 0.26$ s and $T_0 + 0.57$ s with a signal-to-noise ratio (S/N) > 5. Such a signal is clearly identified in the 2-D count map presented in Figure 1. A weaker tail, which is also significant above the background with S/N > 5, appears between $T_0 + 0.95$ s and $T_0 + 1.79$ s. The total span of GRB 170817A is about 2.05 s with a 0.38 s-gap consistent with the background. The burst was also detected in the data of the SPI Anti-Coincidence System (ACS) on-board INTEGRAL [10]. We download the pre-binned (50-ms bin) SPI-ACS light curve from http://isdc.unige.ch/Soft/ibas/ibas_acs_web.cgi, which is derived from 91 independent detectors with different lower energy thresholds (from 60 to 120 keV) and an upper threshold of ~ 10 MeV. The multi-channel GBM light curves and the SPI-ACS light curves are presented in Supplementary Figure S1.

We first extract the time integrated spectrum in the first peak region (i.e., from $T_0 - 0.26$ to $T_0 + 0.57$ s). We select the NaI detectors n1 & n2 and BGO detector b0. The total number of photon counts is significantly above the background counts in NaI detectors. We find the net spectrum can be successfully fitted by a power law function with an exponential high-energy cutoff (hereafter, cutoff power law or CPL model) with the goodness of statistics PGSTAT=263.3 and degree of freedom DOF=363. The power law index is $-0.66^{+0.38}_{-0.54}$ and the cutoff energy, parameterized as E_p ,

□ ¹Instituto de Astrofísica de Andalucía (IAA-CSIC), P.O. Box 03004, E-18080 Granada, Spain; zhang.grb@gmail.com; ²School of Astronomy and Space Science, Nanjing University, Nanjing 210093, China; ³Department of Physics and Astronomy, University of Nevada, Las Vegas, NV 89154, USA; zhang@physics.unlv.edu ⁴Department of Astronomy, School of Physics, Peking University, Beijing 100871, China; ⁵Kavli Institute for Astronomy and Astrophysics, Peking University, Beijing 100871; ⁶National Astronomical Observatories, Chinese Academy of Sciences, A20 Datun Road, Beijing 100012, China; ⁷School of Physics, Huazhong University of Science and Technology, Wuhan 430074, China; ⁸Department of Astronomy, Beijing Normal University, Beijing 100875, China; ⁹Department of Space Sciences and Astronomy, Hebei Normal University, Shijiazhuang 050024, China; ¹⁰Purple Mountain Observatory, Chinese Academy of Sciences, Nanjing 210008, China; ¹¹ Department of Astronomy, University of Florida, 211 Bryant Space Science Center, Gainesville, 32611, USA ¹²Universidad de Granada, Facultad de Ciencias Campus Fuentenueva s/n E-18071 Granada, Spain; ¹³Guangxi Key Laboratory for Relativistic Astrophysics, Department of Physics, Guangxi University, Nanning 530004, China; ¹⁴Joint Center for Particle, Nuclear Physics and Cosmology, Nanjing University-Purple Mountain Observatory, Nanjing 210008, China; ¹⁵School of Physics and Electronics Information, Hubei University of Education, Wuhan 430205, China; ¹⁶Gran Sasso Science Institute (INFN), Via Francesco Crispi 7 LAquila, I-67100, Italy ¹⁷INFN - Sezione di Pisa Edificio C, Largo Bruno Pontecorvo, 3, Pisa, 56127, Italy ¹⁸Departamento de Ingeniería de Sistemas y Automática, Escuela de Ingenierías, Universidad de Málaga, C. Dr. Ortiz Ramos sn, 29071 Málaga, Spain;

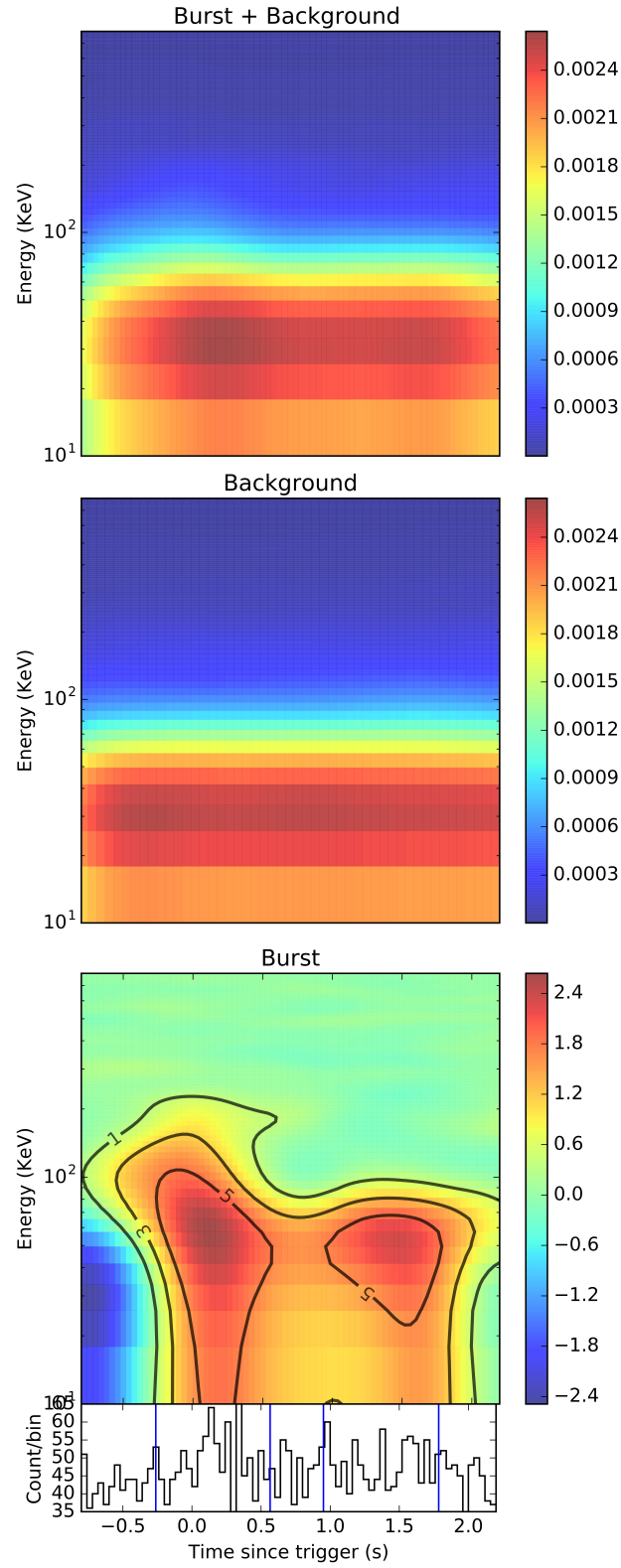


Figure 1: Signal detection from the *Fermi* GBM Time-Tagged Event (TTE) data of GRB 170817A. Top panel shows the observed count map; Middle panel shows the count map in a background region. The background-subtracted count map is presented in the Bottom panel along with the 15-50 keV light curve. The contour lines in the bottom panel represent the levels of signal-to-noise ratio.

TABLE I: Properties of GRB 170817A.

total spanning duration (s)	~ 2.05
spectral peak energy (first peak) E_p (keV)	$158.1^{+180.4}_{-33.7}$
total fluence (erg cm^{-2})	$(4.46 \pm 0.1) \times 10^{-7}$
spectral lag (25-50 keV vs 50-100 keV)	0.03 ± 0.05 s
redshift z	~ 0.009
luminosity distance D_L (Mpc)	39.472
total isotropic energy E_{iso} (erg)	$(4.58 \pm 0.19) \times 10^{46}$
peak luminosity L_{iso} (erg s^{-1})	$(1.7 \pm 0.1) \times 10^{47}$

is $158.1^{+180.4}_{-33.7}$ keV. The corresponding average flux in this time interval is $(2.33 \pm 0.1) \times 10^{-7} \text{ erg cm}^{-2} \text{ s}^{-1}$. The fluence is $(1.93 \pm 0.1) \times 10^{-7} \text{ erg cm}^{-2}$. For the second peak between $T_0 + 0.95$ s and $T_0 + 1.79$ s, we find the net spectrum can be preferably fitted by a blackbody model with $kT = 10.8^{+2.7}_{-1.7}$ keV (PGSTAT/dof=250.9/364). The corresponding average flux in this time interval is $(6.3 \pm 0.3) \times 10^{-8} \text{ erg cm}^{-2} \text{ s}^{-1}$. The fluence is $(5.3 \pm 0.2) \times 10^{-8} \text{ erg cm}^{-2}$. Including both peaks, the total fluence is $(4.46 \pm 0.1) \times 10^{-7} \text{ erg cm}^{-2}$, corresponding to an isotropic energy of $(4.58 \pm 0.19) \times 10^{46} \text{ erg}$. Using a 50 ms time resolution light curve, the peak luminosity at $T_0 \simeq -0.07$ s is derived as $(1.7 \pm 0.1) \times 10^{47} \text{ erg s}^{-1}$. The best-fit parameters are presented in Supplementary Table I. The spectral fitting plots as well as the parameter constraints are presented in Supplementary Figures S2-S4. A mild spectral evolution is observed (Supplementary Figure S5).

We also calculate the spectral lag of the GRB between (25-50) keV and (50-100) keV, which is 0.03 ± 0.05 s, consistent with zero. This is consistent with the spectral lag distribution of sGRBs [14].

With the observed and derivative properties summarized in Table I, one can compare GRB 170817A with other sGRBs. The following samples extracted from the Fermi/GBM catalog [15] are considered for comparison: (1) the long GRB sample with E_p measured (1679 GRBs); (2) the short GRB sample ($T_{90} < 2$ s) with E_p measured (317 GRBs); and (3) the short GRB sample with $S/N < 6$ and E_p measured (66 GRBs). The latter is the faint sGRB sample to which GRB 170817A belongs (Supplementary Figure S6).

We first compare the *observed* properties of GRB 170817A with other GRBs. Figure 2 upper panel is the standard T_{90} –HR (hardness ratio) plot for GRBs. One can see that GRB 170817A falls into the sGRB population, even though in its long and soft regime. Figure 2 lower panel compares GRB 170817A and other GRBs in the fluence vs. E_p diagram. Again GRB 170817A falls into the regime of low fluence and low E_p in the sGRB population. Based on γ -ray information only, this burst would be regarded as one of those normal (but faint and soft) short GRBs if there were no gravitational wave trigger. Comparing the host galaxy NGC 4993 of GRB 170817A with the host galaxies of other sGRBs [3, 16], we find that NGC 4993 falls into the distribution of sGRB hosts in terms of half-light radius, stellar mass, and afterglow offset from the host galaxy (Supplementary Figure S8).

We next investigate the intrinsic property of the burst. Taking into the very small distance $D_L = 39.472$ Mpc of the host galaxy NGC 4993 [17], this burst is abnormally low in terms of luminosity and energy (throughout the paper, luminosity and energy are the isotropic-equivalent ones). The peak isotropic luminosity is $L_{\text{iso}} = (1.7 \pm 0.1) \times 10^{47} \text{ erg s}^{-1}$, and the isotropic energy is $E_{\text{iso}} = (4.58 \pm 0.19) \times 10^{46} \text{ erg}$. Such low-luminosity sGRBs have never been observed before. Plotting it onto the intrinsic peak energy $E_{p,z} = E_p(1+z)$ vs. isotropic energy E_{iso} plane [18], we find that it is within 2σ of the track of the sGRB population, but slightly deviates from the track into the hard regime (Figure 3). The burst would be more normal if the energy increases by two orders of magnitude.

Based on previously known sGRBs, the event rate density (also called volumetric event rate) of sGRBs above then-minimum luminosity ($\sim 10^{50} \text{ erg s}^{-1}$) is a few $\text{Gpc}^{-3} \text{ yr}^{-1}$ [5, 6]. For example, for a Gaussian distribution of the merger delay time [19], the event rate density of sGRBs is $4.2^{+1.3}_{-1.0} \text{ Gpc}^{-3} \text{ yr}^{-1}$ above $7 \times 10^{49} \text{ erg s}^{-1}$ [6]. This is lower than the estimated NS-NS merger event rate density, which is $\sim 10^3 \text{ Gpc}^{-3} \text{ yr}^{-1}$ ([8], see below). The discrepancy may be removed if one considers the beaming correction of sGRBs. Using the inferred beaming factor $f_b \sim 0.04$ inferred from the sparse sGRB jet break data [20], the corrected event rate density (counting for sGRBs not beaming towards us) is $\sim 100 \text{ Gpc}^{-3} \text{ yr}^{-1}$.

With the detection of GRB 170817A, the distribution of the sGRB isotropic peak luminosity extended to a much lower value. The revised event rate density of sGRB above $1.7 \times 10^{47} \text{ erg s}^{-1}$ becomes (Methods)

$$\rho_{0,\text{sGRB}}(L_{\text{iso}} > 1.7 \times 10^{47} \text{ erg s}^{-1}) \geq 190^{+440}_{-160} \text{ Gpc}^{-3} \text{ yr}^{-1}. \quad (1)$$

This is comparable (or somewhat higher) than the previously-derived beaming-corrected sGRB event rate density, but is still a factor of a few smaller than the NS-NS merger event rate density derived based on the detection of GW

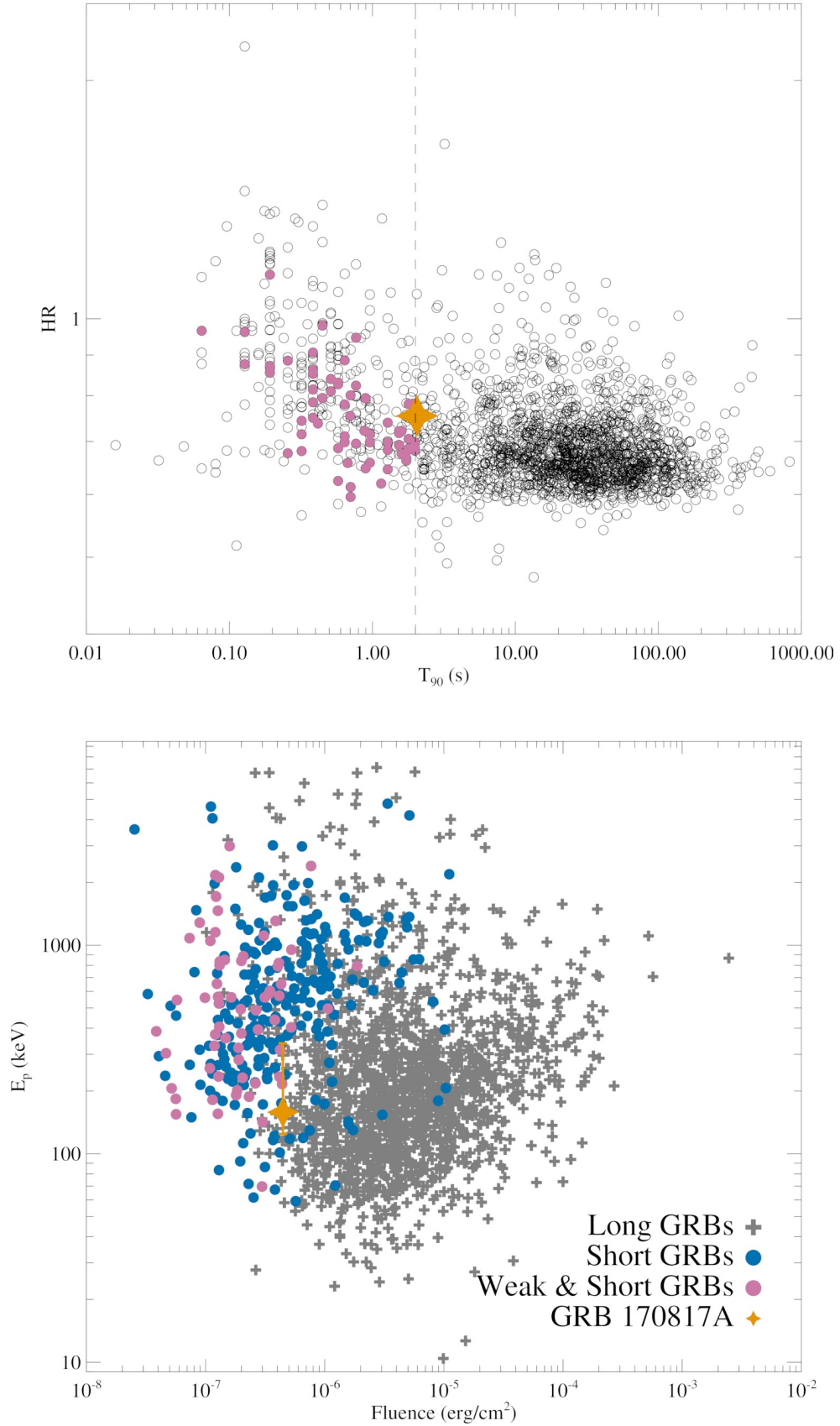


Figure 2: *Upper:* A comparison between GRB 170817A and other Fermi long and short GRBs in the T_{90} –HR diagram. The hardness ratio (HR) is defined as ratio of the observed counts in 50–100 keV band compared to the counts in the 25–50 keV band within the T_{90} region. *Lower:* GRB 170817A in the fluence vs E_p diagram against other sGRBs.

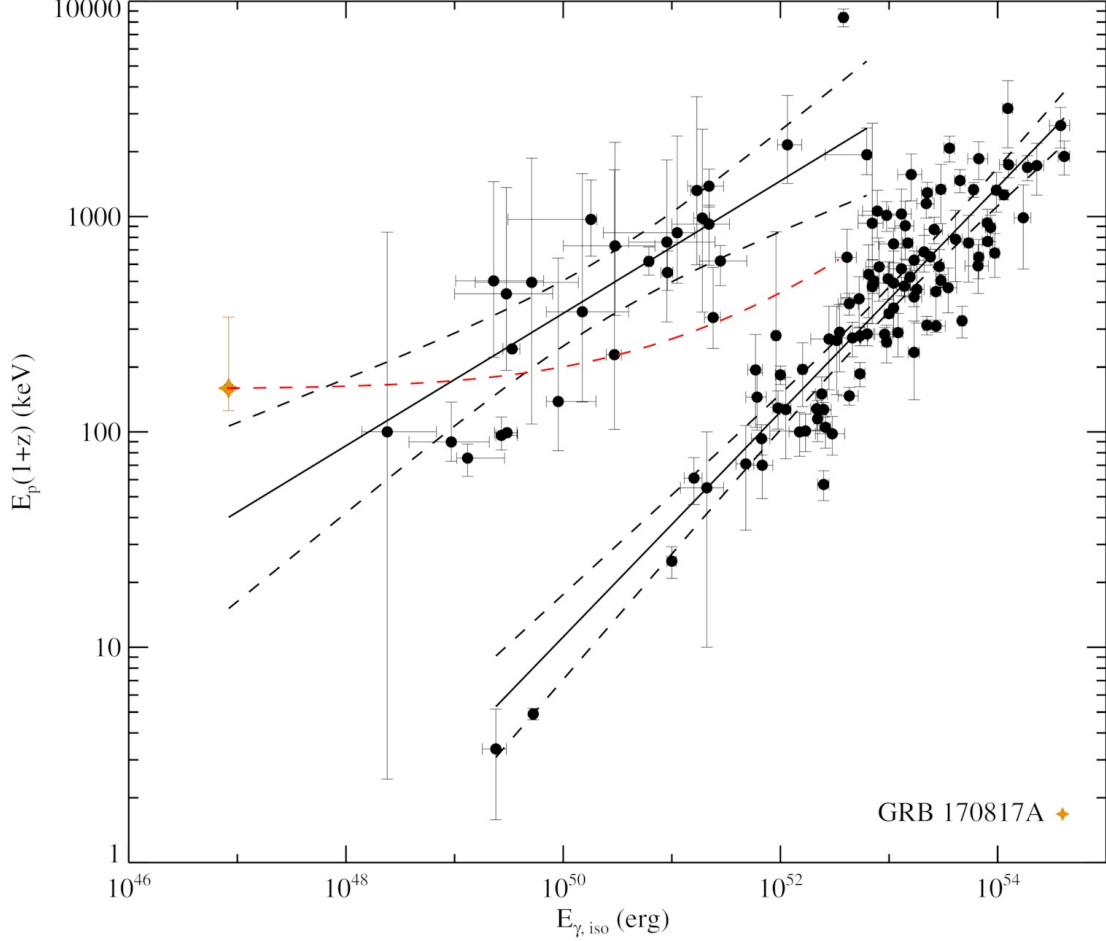


Figure 3: GRB 170817A (orange star) in E_p vs E_{iso} plot. Dashed line represents GRB 170817A position if it were in different redshifts ranging from 0.009 to 3.

170817A [8], which is (Methods)

$$\rho_{0, \text{NS-NS}} = 1100^{+2500}_{-910} \text{ Gpc}^{-3} \text{ yr}^{-1}. \quad (2)$$

Figure 4 upper panel shows the sGRB event rate density as a function of luminosity threshold. The black power-law (PL) line with an index -0.7 was derived from the *Swift* sGRBs (black crosses with error included) with redshift measurements [6]. GRB 170817A (orange) extends the sGRB luminosity by three orders of magnitude in the low- L_{iso} regime. Interestingly, the revised event rate density above $1.7 \times 10^{47} \text{ erg s}^{-1}$ follows the extension of the PL distribution derived by [6]. In view that it is possible that some sGRBs similar to GRB 170817A may be hidden within the GBM archives, the true event rate density could be higher (as high as the NS-NS merger event rate density, blue symbol). In Figure 4 lower panel, we derive a new sGRB luminosity function across a wide range of luminosity, which is consistent with the extrapolation of the previous results that show a power law with $L_{iso}^{-1.7}$ [6].

There are two possibilities to produce a low-luminosity sGRB from an NS-NS merger. The first possibility is a bright sGRB jet viewed off-axis. Within this picture, the main jet (similar to the one observed from a more distant sGRB) beams towards a different direction. However, within such a scenario, one cannot have a sharp-edge conical jet viewed outside the jet cone. This is because the observed duration would be longer than the central engine activity time scale, inconsistent with its typical sGRB duration (Supplementary Information). Rather, one requires a structured jet viewed from a large wing [21, 22] with emission powered by the low-luminosity wind along the line of sight. Within the sGRB context, such a jet configuration has been discussed in terms of a jet-cocoon geometry [23, 24]. A viewing angle $\theta_v \leq 28^\circ$ (or $\leq 36^\circ$ depending on the assumed value of the Hubble constant [31]) has been inferred from the gravitational wave and host galaxy data. This is consistent with such a scenario. Alternatively, the outflow of GRB

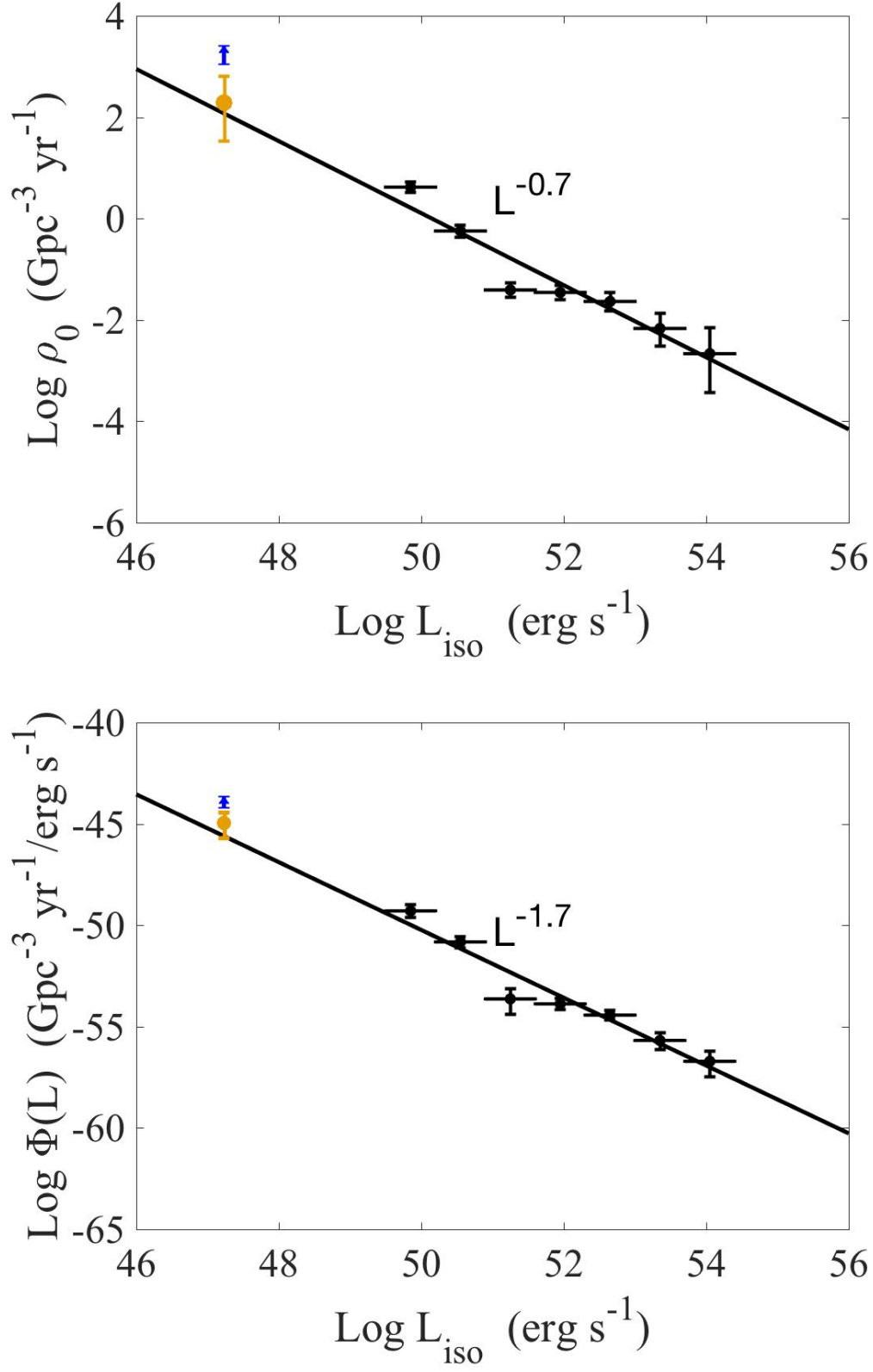


Figure 4: *Upper:* The local event rate density distribution of sGRBs including GRB 170817A. The orange dot denotes the event rate density derived from GRB 170817A and the blue symbol denotes the NS-NS merger event rate density. The black power-law line and dots were derived from *Swift* sGRB sample [6]. The vertical error bar represents the 1σ Gaussian errors. *Lower:* Luminosity function distribution of sGRBs including GRB 170817A, with labels same as the upper panel.

170817A may have an intrinsically low luminosity. Within this picture, not all NS-NS mergers produce energetic jets that power normal sGRBs. The condition of launching an energetic jet may depend on complicated merger physics (e.g. mass in the accretion torus, mass of launched ejecta, magnetic field strength and configuration of the pre- and post-merger objects). In the cases like GRB 170817A, the lack of a bright jet may be due to a very low accretion rate for a black hole post-merger product or a low-magnetic-field post-merger neutron star (Supplementary Information).

With the γ -ray data only, one cannot judge the post-merger product for the NS-NS merger. The short duration of the burst is consistent with a prompt black hole or a hyper-massive neutron star that survived ~ 100 ms before collapsing to a black hole. On the other hand, the amplitude of the short GRB is relatively low, so that the possibility that the burst is the “tip-of-iceberg” of a long-duration event, as expected in the post-merger supra-massive or stable neutron star scenario [25, 26] is not ruled out. We conduct a search of extended emission before and after the trigger time, which leads to a negative result (Supplementary Information). The post-merger gravitational wave signal [27] and the optical transient signal [28] can in principle help to determine the post-merger product. Unfortunately, the post-merger GW signal is not strong enough to make a solid claim of the post-merger product [8]. The optical transient is brighter than the typical luminosity of the predicted kilonova [30]. This may point towards a magnetar engine, even though a black hole engine is not ruled out.

The merger time of the gravitational wave signal is at $T_{GW}=12:41:04.430\pm0.002$ UTC on 17 August 2017 (GPS time $T_{GW}=1187008882.430\pm0.002$ s)[31]. The beginning time of GRB 170817A (~ -0.3 s with respect to the *Fermi*/GBM trigger time $T_0=12:41:06.474598$ UT on 17 August 2017[9]) has a ~ 1.7 s delay with respect to the merger time. It is intriguing that this delay time scale is of the same order as the burst duration. Such a delay offers a diagnostic of the emission site and energy dissipation process of GRBs. In particular, it disfavors the photosphere model which predicts a delay time of milliseconds, but supports the emission models that invoke synchrotron emission in an optically thin region (Supplementary Information).

Assuming a standard radiative efficiency and standard shock microphysics parameters, the low isotropic energy of GRB 170817A suggests that the multi-wavelength afterglows of the burst should be very faint (Supplementary Information). We used the Javier Gorosabel 0.6m robotic telescope at the BOOTES-5 station at Observatorio Nacional de San Pedro Martir (Mexico) to image the 15 galaxies in the GLADE Catalogue starting on Aug 18.21 UT. The optical counterpart (SSS17a) of GW 170717 was detected in the outskirts of the NGC 4993 galaxy, with a magnitude $R = 18.20 \pm 0.45$, in agreement with other contemporaneous measurements. This is much brighter than the predicted flux of optical afterglow. As a result, this optical transient should originate from a quasi-thermal kilonova [29, 30] or mergernova [28].

Within the Fermi GBM soft faint sGRB sample, there might be some GRB 170817A-like events. Some events are presented in Supplementary Figure S7. Placing an upper limit based on the NS-NS merger event rate density, we estimate that there might be at most a few more similar events in the entire sample (Supplementary Information). However, identifying them turns out difficult without gravitational wave detections (Supplementary Information).

References

-
1. Eichler, D., Livio, M., Piran, T., & Schramm, D. N. Nucleosynthesis, neutrino bursts and gamma-rays from coalescing neutron stars. *Nature* **340**, 126-128 (1989)
 2. Gehrels, N., et al. A short γ -ray burst apparently associated with an elliptical galaxy at redshift $z = 0.225$. *Nature* **437**, 851-854 (2005)
 3. Fong, W., Berger, E., & Fox, D. B. Hubble Space Telescope Observations of Short Gamma-Ray Burst Host Galaxies: Morphologies, Offsets, and Local Environments. *Astrophys. J.* **708**, 9-25 (2010)
 4. Berger, E. Short-Duration Gamma-Ray Bursts. *Annu. Rev. Astron. Astr.* **52**, 43-105 (2014)
 5. Wanderman, D., & Piran, T. The rate, luminosity function and time delay of non-Collapsar short GRBs. *Mon. Not. R. Astron. Soc.* **448**, 3026-3037 (2015)
 6. Sun, H., Zhang, B., & Li, Z. Extragalactic High-energy Transients: Event Rate Densities and Luminosity Functions. *Astrophys. J.* **812**, 33 (2015)
 7. Ghirlanda, G., et al. Short gamma-ray bursts at the dawn of the gravitational wave era. *Astron. Astroph.* **594**, A84 (2016)
 8. Abbott, B. P. et al. (LIGO Scientific Collaboration and Virgo Collaboration) GW 170817: Observation of gravitational waves from a binary neutron star inspiral. *Phys. Rev. Lett.*, **119**, 161101 (2017).
 9. Goldstein et al. An ordinary short gamma-ray burst with extraordinary implications: Fermi/GBM detection of GRB 170817A, *Astrophys. J. Lett.*, **848**, L14 (2017).
 10. Savchenko, V., et al., INTEGRAL detection of the first prompt gamma-ray signal coincident with the gravitational wave event GW170817, *Astrophys. J. Lett.*, **848**, L15 (2017).

11. Coulter, D. et al. Swope Supernova Survey 2017a (SSS17a), the optical counterpart to a gravitational wave source. *Science*, <https://doi.org/10.1126/science.aap9811> (2017).
12. Meegan, C., et al. The Fermi Gamma-ray Burst Monitor. *Astrophys. J.* **702**, 791-804-(2009)
13. Zhang, B.-B., Uhm, Z. L., Connaughton, V., Briggs, M. S., & Zhang, B. Synchrotron Origin of the Typical GRB Band Function – A Case Study of GRB 130606B. *Astrophys. J.* **816**, 72 (2016)
14. Gehrels, N., et al. A new γ -ray burst classification scheme from GRB060614. *Nature* **444**, 1044-1046 (2006)
15. Narayana Bhat, P., et al., The Third Fermi GBM Gamma-Ray Burst Catalog: The First Six Years, *Astrophys. J. Suppl. S.* **223**, 28, (2016)
16. Li, Y., Zhang, B., & Lü, H.-J. A Comparative Study of Long and Short GRBs. I. Overlapping Properties. *Astrophys. J. Suppl. S.* **227**, 7-(2016)
17. Koppapapu, R. K., Hanna, C., Kalogera, V., O’Shaughnessy, R., González, G., Brady, P. R., & Fairhurst, S. Host Galaxies Catalog Used in LIGO Searches for Compact Binary Coalescence Events. *Astrophys. J.* **675**, 1459-1467(2008)
18. Amati, L., et al. Intrinsic spectra and energetics of BeppoSAX Gamma-Ray Bursts with known redshifts. *Astron Astrophys.* **390**, 81-89 (2002)
19. Virgili, F.J., et al., Are All Short-hard Gamma-ray Bursts Produced from Mergers of Compact Stellar Objects? *Astrophys. J.* **727**, 109, (2011).
20. Fong, W., Berger, E., Margutti, R., & Zauderer, B. A., A Decade of Short-duration Gamma-Ray Burst Broadband Afterglows: Energetics, Circumburst Densities, and Jet Opening Angles, *Astrophys. J.* **815**, 102, (2015)
21. Zhang, B. and Mészáros, P., Gamma-Ray Burst Beaming: A Universal Configuration with a Standard Energy Reservoir? *Astrophys. J.* **571**, 876-879 (2002).
22. Rossi, E., Lazzati, D., and Rees, M.J., Afterglow light curves, viewing angle and the jet structure of γ -ray bursts, *Mon. Not. R. Astron. Soc.* **332**, 945, (2002).
23. Lamb, G.P and Kobayashi, S., Electromagnetic Counterparts to Structured Jets from Gravitational Wave Detected Mergers, *ArXiv e-prints*, arXiv:1706.03000, (2017).
24. Lazzati, D., et al., Off-axis emission of short γ -ray bursts and the detectability of electromagnetic counterparts of gravitational-wave-detected binary merger, *Mon. Not. R. Astron. Soc.* **471**, 1652, (2017).
25. Zhang, B., Early X-Ray and Optical Afterglow of Gravitational Wave Bursts from Mergers of Binary Neutron Stars, *Astrophys. J.* **763**, L22, (2013)
26. Sun, H., Zhang, B., and Gao, H. X-Ray Counterpart of Gravitational Waves Due to Binary Neutron Star Mergers: Light Curves, Luminosity Function, and Event Rate Density, *Astrophys. J.* **835**, 7, (2017)
27. Rezzolla, L. and Takami, K., Gravitational-wave signal from binary neutron stars: A systematic analysis of the spectral properties, *Phys. Rev. D* **93**, 124051, (2016).
28. Yu, Y.-W., Zhang, B., Gao, H., Bright “Merger-nova” from the Remnant of a Neutron Star Binary Merger: A Signature of a Newly Born, Massive, Millisecond Magnetar, *Astrophys. J.* **776**, L40, (2013).
29. Li, L.-X., & Paczyński, B., Transient Events from Neutron Star Mergers, *Astrophys. J.* **507**, L59, (1998)
30. Metzger, B. D., et al., Electromagnetic counterparts of compact object mergers powered by the radioactive decay of r-process nuclei, *Mon. Not. R. Astron. Soc.* **406**, 2650, (2010)
31. Abbott, B. P. et al. (LIGO Scientific Collaboration and Virgo Collaboration) Gravitational Waves and Gamma Rays from a Binary Neutron Star Merger: GW170817 and GRB 170817A, *Astrophys. J. Lett.* **848**, L13 (2017).

Correspondence and requests for materials should be addressed to BBZ (zhang.grb@gmail.com) and BZ (zhang@physics.unlv.edu).

Acknowledgments

We acknowledge the use of the public data from the *Fermi* and *INTEGRAL* data archives. BBZ and AJCT acknowledge support from the Spanish Ministry Projects AYA 2012-39727-C03-01 and AYA2015-71718-R. BZ, WHL, HG, XFW, LS and EWL are supported by the 973 program under grant 2014CB845800. BZ, HS, HG and XFW are supported by the Strategic Priority Research Program of the Chinese Academy of Sciences “Multi-waveband Gravitational Wave Universe”(Grant No. XDB23040000). HG acknowledges the National Natural Science Foundation of China under grants No. 11722324, 11603003, 11633001 and 11690024. HJL acknowledges the National Natural Science Foundation of China under grants 11603006. YDH acknowledges the support by China Scholarships Council (CSC) under the Grant No.201406660015. XYW acknowledges the National Natural Science Foundation of China under grant 11625312. LS acknowledges the supported by the Joint NSFC-ISF Research Program (No. 11361140349), jointly funded by the National Natural Science Foundation of China and the Israel Science Foundation. XF was supported by Natural Science Foundation of China under Grants No. 11673008. The BOOTES-5/JGT observations were carried out at observatories Astronomico Nacional in San Pedro Martir (OAN-SPM, Mexico), operated by Instituto de Astronomia, UNAM and with support from Consejo Nacional de Ciencia y Tecnologia (Mexico) through the Laboratorios Nacionales Program (Mexico), Instituto de Astrofisica de Andalucia (IAA-CSIC, Spain) and Sungkyunkwan University (SKKU, South Korea). We thank the staff of OAN-SPM for their support in carrying out the observations.

METHODS

sGRB event rate density The abnormally low luminosity and extremely small distance of GRB 170817A suggest that the actual event rate density of short GRBs is large. With one detection, we can estimate the local event rate density $\rho_{0,\text{sGRB}}$ of short GRBs through

$$N_{\text{sGRB}} = \frac{\Omega_{\text{GBM}} T_{\text{GBM}}}{4\pi} \rho_{0,\text{sGRB}} V_{\text{max}} \geq 1 \quad (3)$$

The field of view of GBM is approximatively taken as full sky with $\Omega_{\text{GBM}} \simeq 4\pi$. The working time of GBM is taken since 2008 with a duty cycle of $\sim 50\%$, so that $T_{\text{GBM}} \simeq 4.5\text{yrs}$. The maximum volume a telescope can detect for this low luminosity event is $V_{\text{max}} = 4\pi D_{\text{L,max}}^3/3$. We simulate a set of pseudo-GRBs by placing GRB 170817A to progressively larger distances, and find that the signal would not be detectable at 65 Mpc (Supplementary Information). Taking this distance as $D_{\text{L,max}}$, we derive the event rate density of sGRBs [6]

$$\rho_{0,\text{sGRB}}(L_{\text{iso}} > 1.7 \times 10^{47} \text{erg s}^{-1}) \geq 190_{-160}^{+440} \text{ Gpc}^{-3} \text{yr}^{-1}. \quad (4)$$

The event rate density of NS-NS mergers may be also estimated based on one detection by aLIGO during O1 and O2. Since only one NS-NS merger event was detected [8], one may write

$$N_{\text{NS-NS}} = \frac{\Omega_{\text{LVC}}}{4\pi} \rho_{0,\text{NS-NS}} (V_{\text{max,O1}} T_{\text{O1}} + V_{\text{max,O2}} T_{\text{O2}}) = 1. \quad (5)$$

Noticing $\Omega = 4\pi$ for GW detectors, taking NS-NS merger horizon ~ 60 Mpc and ~ 80 Mpc for O1 and O2, respectively, and adopting a duty cycle of $\sim 40\%$ for both O1 and O2, we estimate

$$\rho_{0,\text{NS-NS}} = 1100_{-910}^{+2500} \text{ Gpc}^{-3} \text{yr}^{-1}. \quad (6)$$

This is consistent with the NS-NS merger event rate density derived by the LIGO team using more sophisticated simulations [8]. This rate is greater than the event rate density of GRB 170817A-like events. This either suggests that there might be even less luminous sGRBs than GRB 170817A, or there might be similar sGRBs hidden in the GBM archives that are associated with NS-NS mergers. The number of these events is at most a few.

Supplementary Information

1. Detailed light curves and spectral fit to GRB 170817A

The multi-channel light curves observed by Fermi/GBM and INTEGRAL/SPI-ACS is presented in Supplementary Figure S1.

As discussed in the main text, a cutoff power law presents an adequate fit to the spectral data. The best fitting result for the time interval ($T_0 - 0.26, T_0 + 0.57$) is presented in Supplementary Figure S2. We noticed that a simple power law model can also fit the data with a power law index $-1.74^{+0.08}_{-0.13}$ and PGSTAT/dof 272.6/364. To check whether the cutoff power law fit is overfitting (since it has one extra parameter), we employ a Bayesian information criterion (BIC) [32] to check its statistical evidence. As shown in Supplementary Table S1, the comparison of the two models leads to $\Delta\text{BIC} = 3.35$ (cutoff power law model has the lower BIC). As suggested by [32], such a ΔBIC value indicates positive evidence against the model with a higher BIC (Power Law model in this case). So we favorably choose the cutoff power law model throughout our analysis.

We also compare the fits between the blackbody (BB) model and the CPL model. For the time-integrated spectral fitting, according to BIC, the BB model is less preferred to fit the observed spectra. We also notice the best-fit low energy photon index -0.66 in the CPL model is too soft to match the blackbody value ($+1$). Indeed as shown in Supplementary Figure S3, the deviation of the BB model from the data in the low energy regime is apparent.

According to BIC, the weaker emission between 0.95 s and 1.79 s is favorably fitted by the BB model with $kT = 10.82^{+2.65}_{-1.65}$ keV. The best fitting result this time interval is presented in Supplementary Figure S4.

Due to the low number of photon counts and short duration, the finest bin size we are able to perform a time-resolved spectral analysis is around 0.2-0.3 s, below which the spectral parameters become unconstrained. We select the brightest region between $T_0 - 0.3$ s and $T_0 + 0.4$ s in the first peak, divide it into two equal slices, and perform the time-dependent spectral analysis on them. We present the spectral evolution properties in Supplementary Table S1 and Supplementary Figure S5. Our analysis suggests that there are indeed some spectral differences between the two slices.

We also test the multi-color blackbody (mBB) model in each time interval. As shown in Supplementary Table S1, such a mBB model is not preferred against either the CPL or the BB model. We thus regard that the mBB model is not demanded by the data and using it would overfit the data.

2. Definition of The Faint Short GRB Sample

In Supplementary Figure S6, we plot all the Fermi GBM short GRBs in terms of their signal-to-noise ratio (S/N), fluence, and E_p . The bin where GRB 170817A is located in is marked as the red dashed vertical line. The sample to the left of the line in the S/N plot is defined as the faint sGRB sample. We plot some examples of the light curves of this sample in Supplementary Figure S7.

3. NGC 4993 as a sGRB host

The host galaxy NGC 4993 of GRB 170817A is an elliptical galaxy in the constellation Hydra. In Supplementary Figure S8 left panel we plot the half light radius R_{50} and stellar mass M_* of NGC 4993 against those of other short GRBs ([16] and references therein). It is found that NGC 4993 falls in the middle of the distributions and can be regarded as a typical short GRB host. The optical transient SSS17a has a projected distance of $10.6''$ from the center of NGC 4993. We plot the physical and normalized offset of this event and compare it with other sGRBs (Supplementary Figure S8 right panel). Again, it is consistent with other sGRBs.

4. The maximum detectable distance of GRB 170817A

In order to check at what distance GRB 170817A will become undetectable, we simulate several light curves in 15-350 keV by placing the burst at progressively larger distances from 45 to 80 Mpc. The background level is assumed to be the unchanged. The source count rate is assumed to scale as D_L^{-2} . A $1-\sigma$ Poisson noise was added in each simulation. Our simulation suggests that the burst will become hardly detected at $D_L \simeq 65$ Mpc (Supplementary Figure S9). We therefore adopt this value as $D_{L,\text{max}}$ to estimate the event rate density of GRB 170817A-like GRBs.

5. Amplitude parameter and possible underlying emission

[33] defined an amplitude parameter f , which is the ratio between the peak flux and average background flux of a burst. They found that the f parameter can be used to search for disguised short GRBs due to the “tip-of-iceberg” effect. Arbitrarily raising the background flux, one can always reduce the duration of a long GRB until its measured duration is shorter than 2 s. The amplitude parameter for such a pseudo GRB was defined as f_{eff} by [33]. Comparing the f values of short GRBs and f_{eff} values of long GRBs, [33] found that most short GRBs have an f value that is large enough (say, above 2) so that they are genuine. Performing the same analysis to GRB 170817A, we find that its amplitude parameter is small, i.e. $f \sim 1.43$. As shown in Supplementary Figure S10, this value (red star) is smaller than most short GRBs, and can be confused as a disguised sGRB. The probability (p) for it to be a disguised sGRB is $p \sim 0.17$ according to the $p-f$ relation derived by [33]. Even though the probability for an intrinsically short duration is higher, the probability that the intrinsic duration is long is not negligible. One cannot rule out the possibility that

TABLE S1: Spectral Fitting Results of GRB 170817A

Time	Cutoff Power-Law Fitting		Power-Law Fitting		Blackbody Fitting		mBB Fitting		Model Comparison					
$t_1 \sim t_2$ (s)	α	E_p (keV)	$\frac{EGSTAT}{dof}$	α	$\frac{EGSTAT}{dof}$	kT (keV)	$\frac{EGSTAT}{dof}$	kT _{min} (keV)	kT _{max} (keV)	m	$\frac{EGSTAT}{dof}$	BIC _{pl} - BIC _{cpl}	BIC _{bb} - BIC _{cpl}	BIC _{mbb} - BIC _{bb}
-0.26 ~ 0.57	-0.66 $^{+0.38}_{-0.57}$	158.1 $^{+180.4}_{-55.4}$	263.3/363	-1.61 $^{+0.08}_{-0.69}$	272.6/364	26.0 $^{+10.8}_{-14.3}$	272.2/364	7.3 $^{+6.9}_{-5.5}$	105.3 $^{+218.2}_{-172.9}$	-0.65 $^{+0.23}_{-0.88}$	262.3/362	3.35	2.96	4.84
-0.3 ~ 0.05	0.18 $^{+1.33}_{-1.18}$	158.8 $^{+593.5}_{-32.1}$	245.0/363	-1.67 $^{+0.69}_{-0.78}$	255.2/364	35.3 $^{+6.5}_{-6.5}$	245.6/364	10.3 $^{+38.7}_{-8.9}$	58.8 $^{+172.9}_{-17.3}$	-0.76 $^{+0.88}_{-1.16}$	245.1/362	4.3	-5.3	6.0
0.05 ~ 0.4	-0.84 $^{+1.18}_{-0.68}$	61.3 $^{+133.5}_{-179.3}$	215.4/363	-2.12 $^{+0.19}_{-0.83}$	218.8/364	10.6 $^{+11.7}_{-2.85}$	217.5/364	6.6 $^{+60.1}_{-1.8}$	54.3 $^{+230.3}_{-40.7}$	-1.50 $^{+2.21}_{-0.23}$	215.4/362	2.5	-3.8	5.9
0.95 ~ 1.79	3.97 $^{+0.02}_{-2.15}$	40.0 $^{+179.4}_{-4.0}$	250.3/363	-2.15 $^{+0.3}_{-2.3}$	261.0 / 364	10.82 $^{+2.85}_{-1.65}$	250.95/364	unconstrained	unconstrained			4.7	-5.3	-

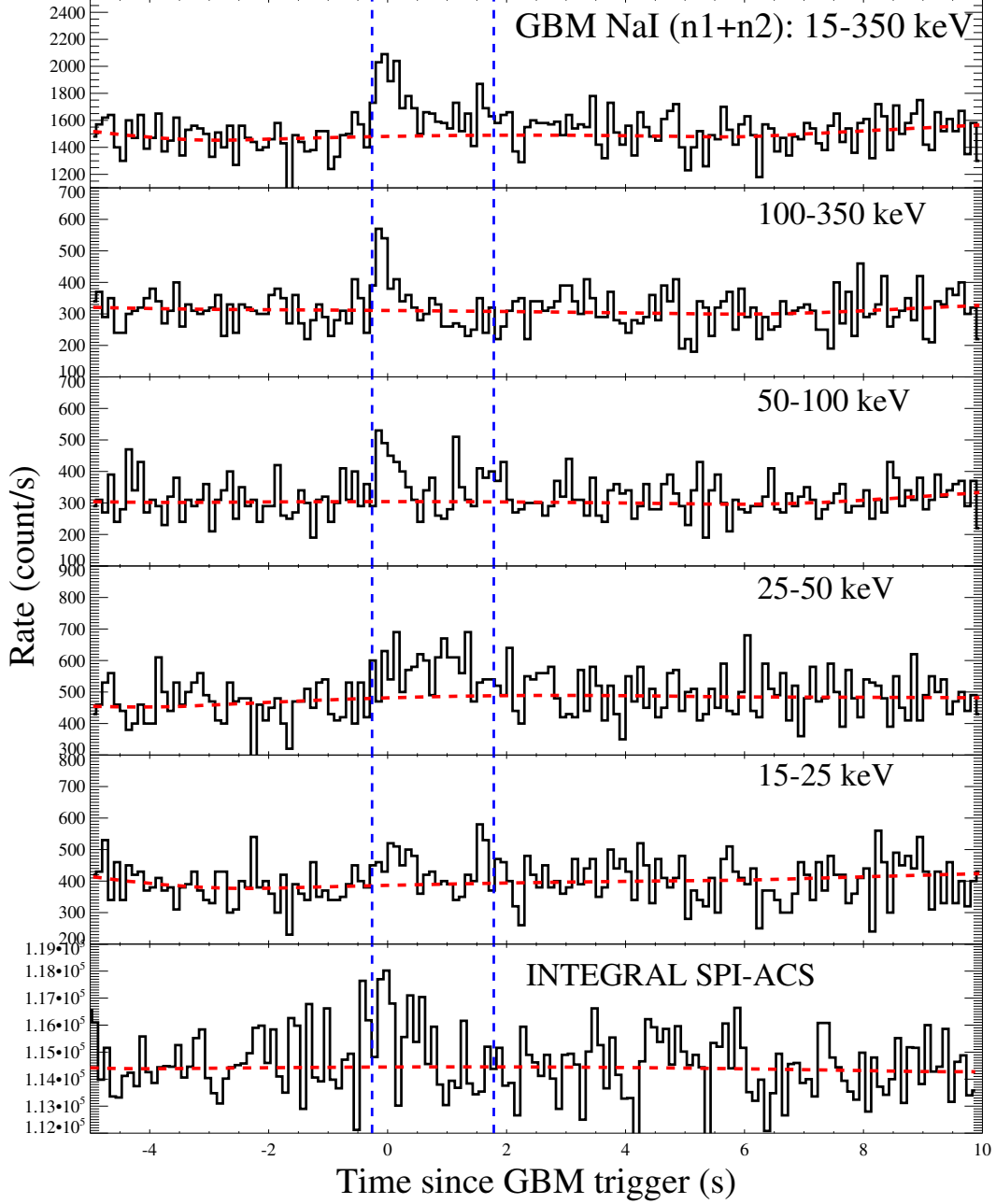


Figure S1: Multi-Channel Light Curves observed by *Fermi*/GBM and *INTEGRAL*/SPI-ACS. The two vertical dashed lines indicate the $S/N > 5$ region as shown in Figure 1.

there is an underlying, weak, long-duration emission component below the background.

In order to search for a possible signal before and after the burst, we perform a detailed spectral analysis in the following time intervals: $-2.0 \sim -1.4$, $-1.4 \sim -0.8$, $4.0 \sim 13.2$, $13.2 \sim 22.4$, $22.4 \sim 31.6$, $31.6 \sim 40.8$, and $40.8 \sim 50.0$ seconds. We do not find any significant emission above the background in any of these time intervals and the spectral fitting performed in these intervals simply give overfit/unconstrained parameters.

6. Off-axis model

For a uniform jet with sharp edge viewed outside the jet cone, the observed duration is different from the observed duration of an on-beam observer, given the same central engine activity time scale. The ratio between the two times

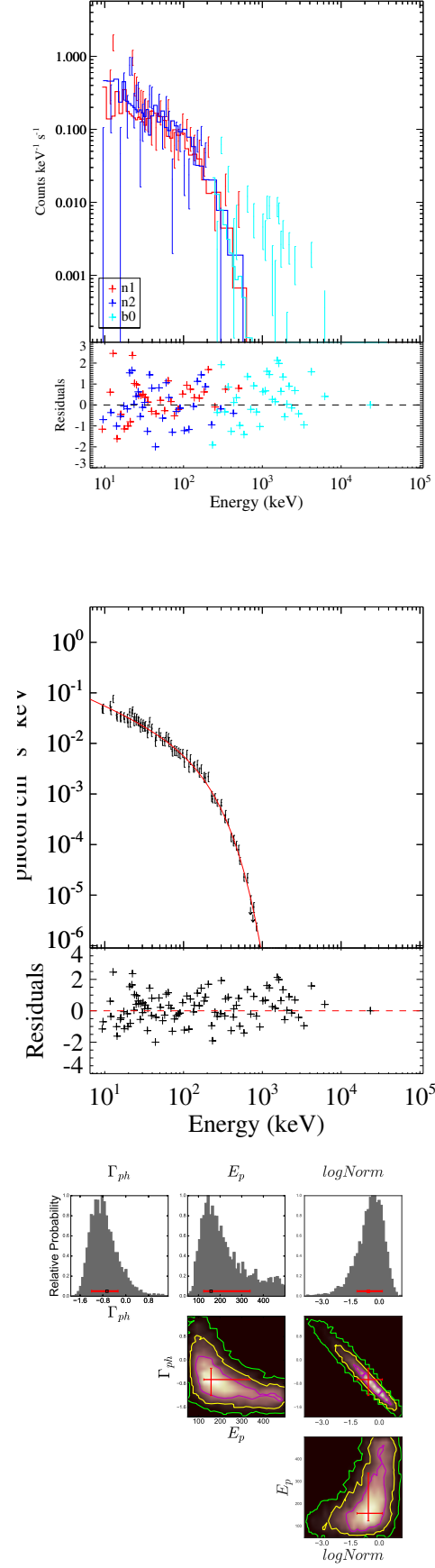


Figure S2: Spectral fitting result for the interval $(T_0 - 0.26, T_0 + 0.57)$. From top to bottom: count spectrum, de-convolved photon spectrum and parameter likelihood map.

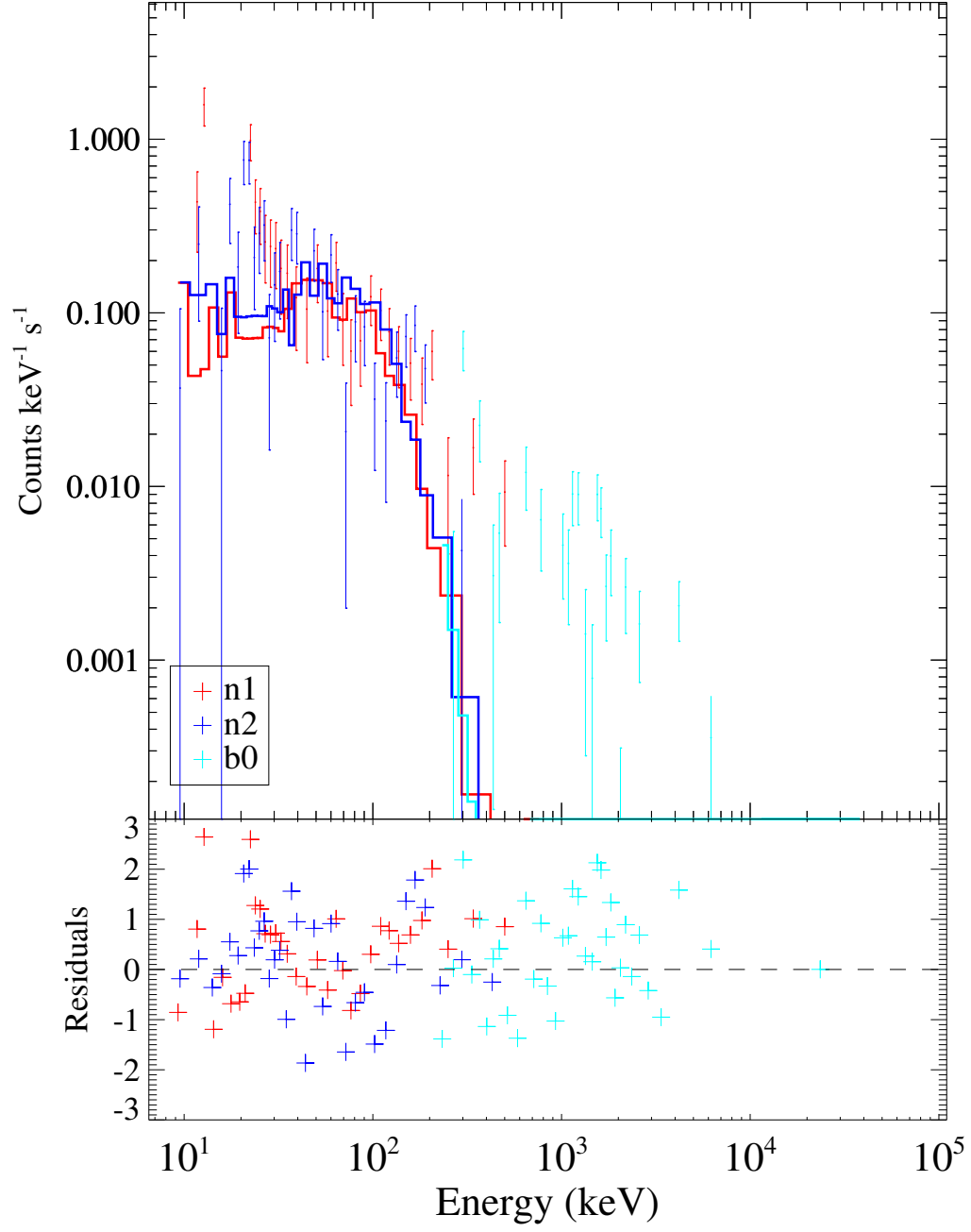


Figure S3: Single blackbody fit for the integrated spectrum between $T_0 - 0.26$ s and $T_0 + 0.57$ s. The deviation in the low energy part is obvious.

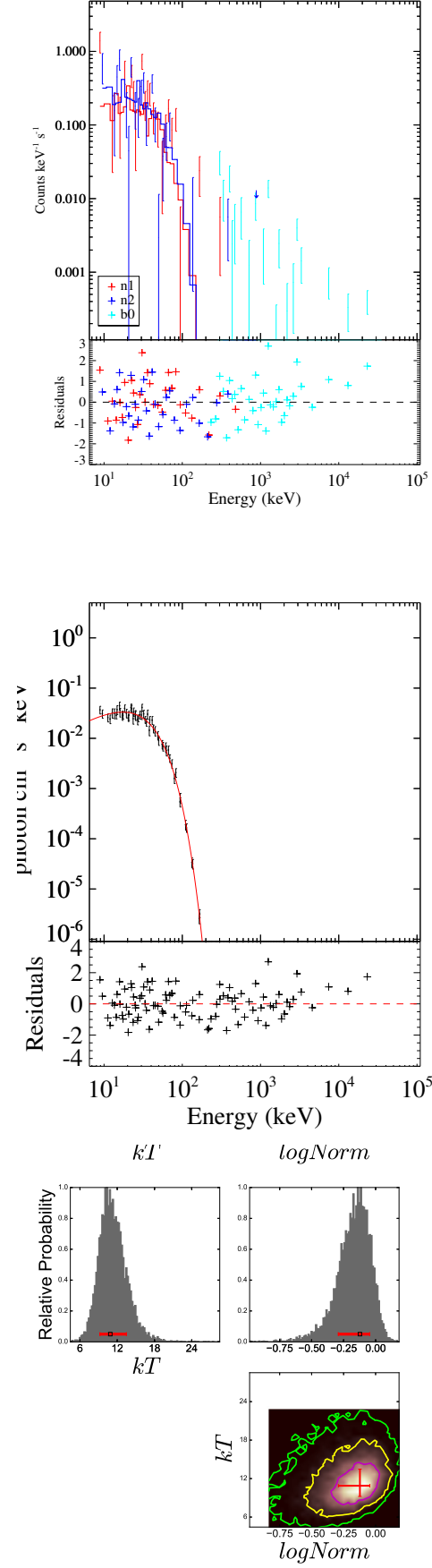


Figure S4: Spectral fitting result for the interval $(T_0 + 0.95, T_0 + 1.79)$ s. From top to bottom: count spectrum, de-convolved photon spectrum and parameter likelihood map.

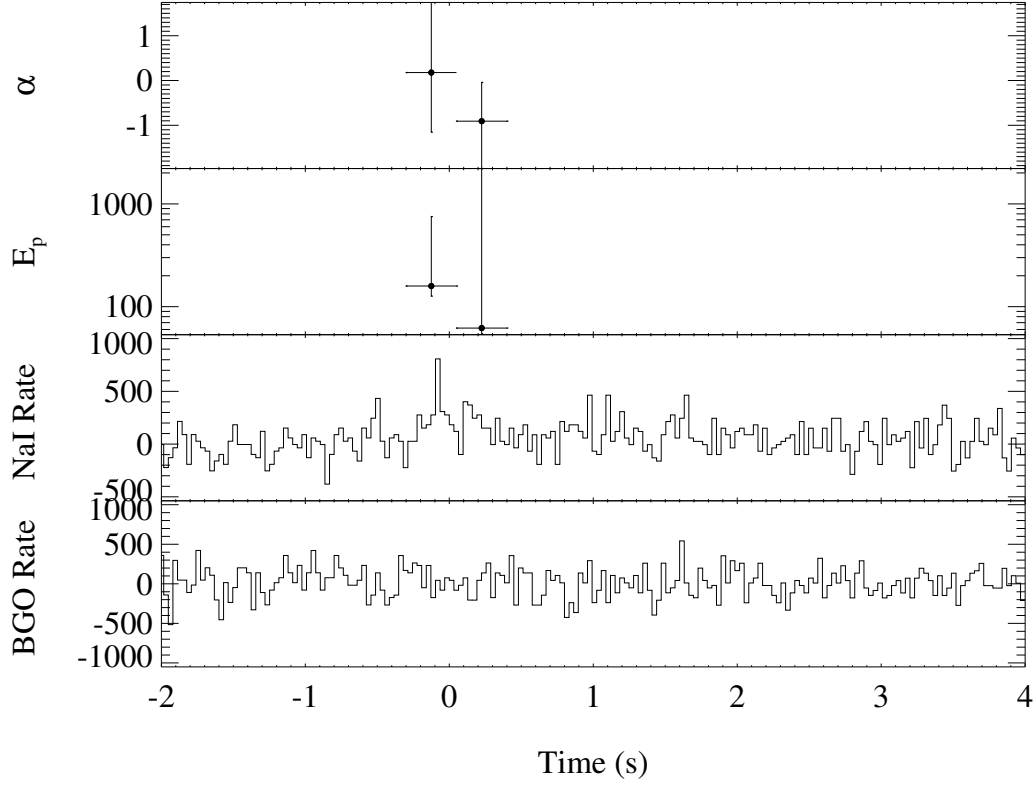


Figure S5: Spectral evolution of the burst. Top two panels show evolution of the photon index (α) and peak energy (E_p). Bottom two panels show the NaI (n1) light curve in 15-350 keV and BGO light curve in 250- 20000 keV.

reads [34]

$$\frac{t(\text{off} - \text{beam})}{t(\text{on} - \text{beam})} = \frac{\mathcal{D}(\theta = 0)}{\mathcal{D}(\theta = \theta_v - \theta_j)} = \frac{1 - \beta \cos(\theta_v - \theta_j)}{1 - \beta}, \quad (7)$$

where θ_j is the jet opening angle, θ_v is the viewing angle from the jet axis, $\mathcal{D} = 1/\Gamma(1 - \beta \cos \theta)$ is the Doppler factor, β is the dimensionless velocity, Γ is the Lorentz factor, and θ is the angle from the line-of-sight. Since the on-beam Doppler factor can be much larger than the off-beam one, the off-beam duration can be much longer than the on-beam one. The observed ~ 2.05 s duration therefore argues against such a possibility. A structured jet invokes on-beam ejecta along the line-of-sight, albeit with a much lower luminosity than that near the jet axis [21, 22]. The observed duration in this case tracks the central engine activity just like the on-beam case. Therefore the off-axis structured jet is consistent with the data.

7. Intrinsically low-luminosity model - a black hole engine

If the sGRB jet is powered by accretion onto a newly formed post-merger black hole, there could be two types of jet launching mechanisms.

First, the Blandford-Znajek [35] mechanism powers a jet from a BH with mass M_\bullet and angular momentum J_\bullet is [36–38]

$$\begin{aligned} \dot{E}_B &= 1.7 \times 10^{50} a_\bullet^2 m_\bullet^2 B_{\bullet,15}^2 F(a_\bullet) \text{ erg s}^{-1} \\ &\simeq 9 \times 10^{53} a_\bullet^2 \dot{m} X(a_\bullet) \text{ erg s}^{-1}, \end{aligned} \quad (8)$$

where $a_\bullet = J_\bullet c / G M_\bullet$ is the BH spin parameter, and $\dot{m} = \dot{M} / 1 M_\odot \text{ s}^{-1}$ is the dimensionless accretion rate, $m_\bullet = M_\bullet / M_\odot$ and $B_{\bullet,15} = B_\bullet / 10^{15} \text{ G}$. Here $F(a_\bullet) = [(1 + q^2)/q^2][(q + 1/q) \arctan q - 1]$, $q = a_\bullet / (1 + \sqrt{1 - a_\bullet^2})$, and $X(a_\bullet) = F(a_\bullet) / (1 + \sqrt{1 - a_\bullet^2})^2$.

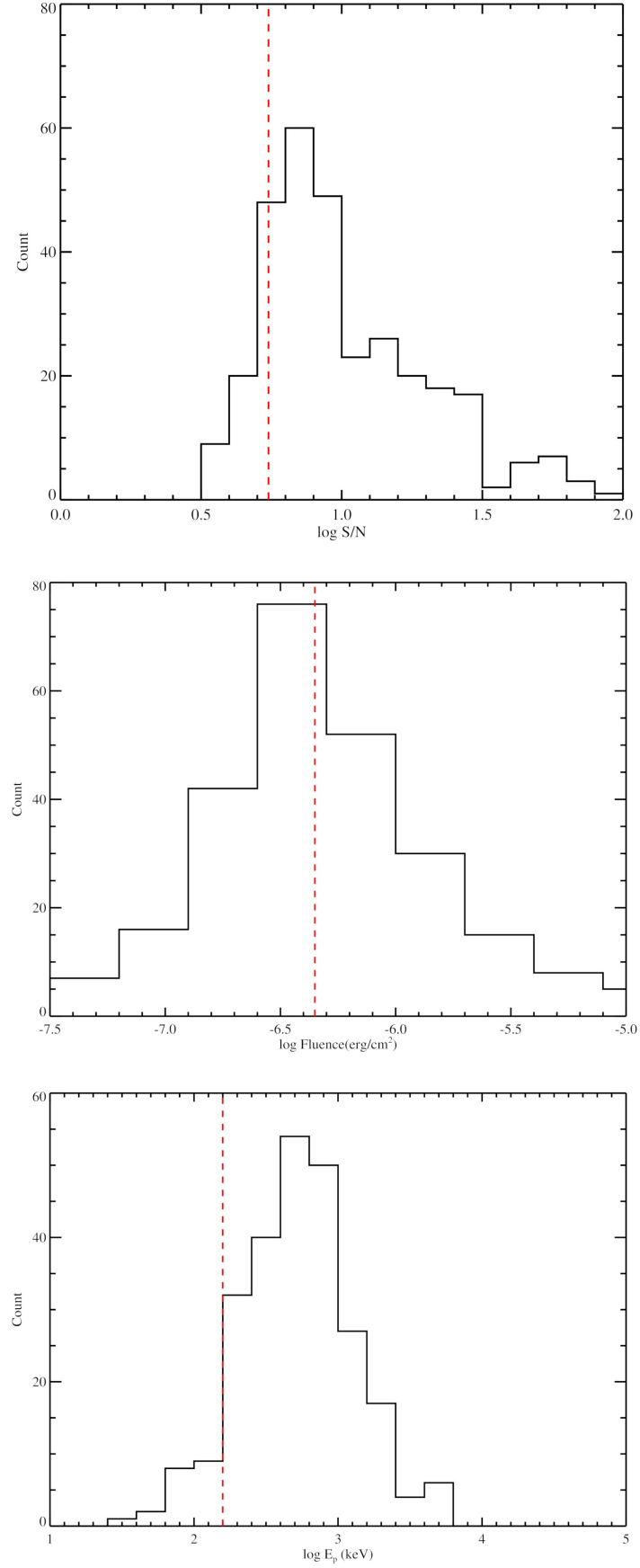


Figure S6: The Fermi GBM short GRB histograms in terms of S/N ratio distribution, fluence distribution, and E_p distribution. The vertical red lines indicate the values for GRB 170817A.

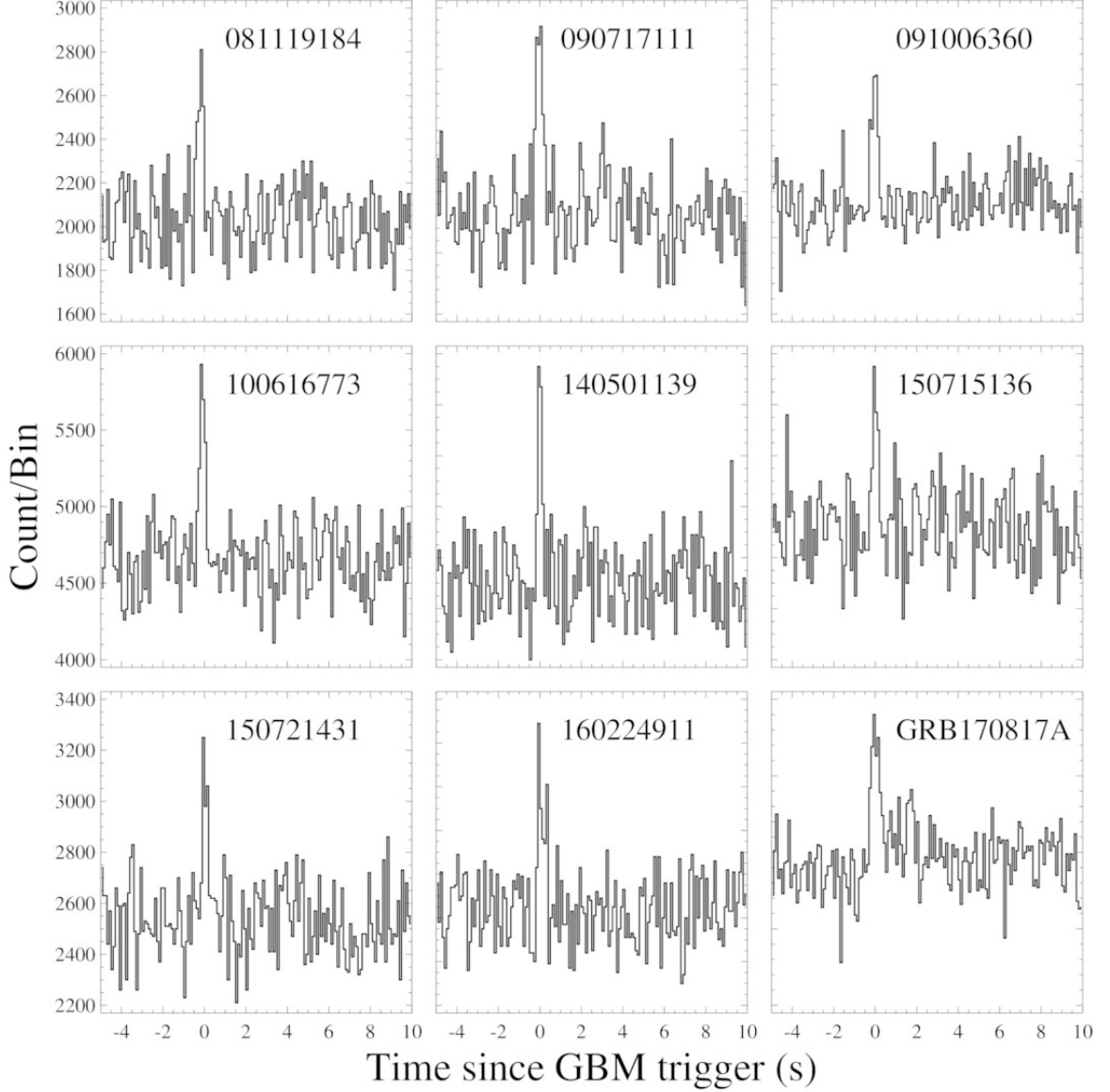


Figure S7: Light curve examples for other GRB 170817A-like events.

For a burst with peak luminosity $L_{\gamma, \text{iso}} \simeq 1.7 \times 10^{47} \text{ erg s}^{-1}$, the magnetic field will be of order of $\sim 5.5 \times 10^{12} \text{ G}$ or accretion rate of $\dot{m} \simeq 1.5 \times 10^{-7}$ for a BZ model with $m_{\bullet} = 3$, $a_{\bullet} = 0.7$, jet beaming factor $f_b \sim 0.01$ and efficiency of $\eta \sim 0.1$.

Alternatively, the jet may be launched via neutrino-anti-neutrino annihilations [39–42]. The neutrino annihilation power can be estimated by [43, 44],

$$\begin{aligned} \dot{E}_{\nu\bar{\nu}} \simeq & \dot{E}_{\nu\bar{\nu}, \text{ign}} \left[\left(\frac{\dot{m}}{\dot{m}_{\text{ign}}} \right)^{-\alpha_{\nu\bar{\nu}}} + \left(\frac{\dot{m}}{\dot{m}_{\text{ign}}} \right)^{-\beta_{\nu\bar{\nu}}} \right]^{-1} \\ & \times \left[1 + \left(\frac{\dot{m}}{\dot{m}_{\text{trap}}} \right)^{\beta_{\nu\bar{\nu}} - \gamma_{\nu\bar{\nu}}} \right]^{-1}, \end{aligned} \quad (9)$$

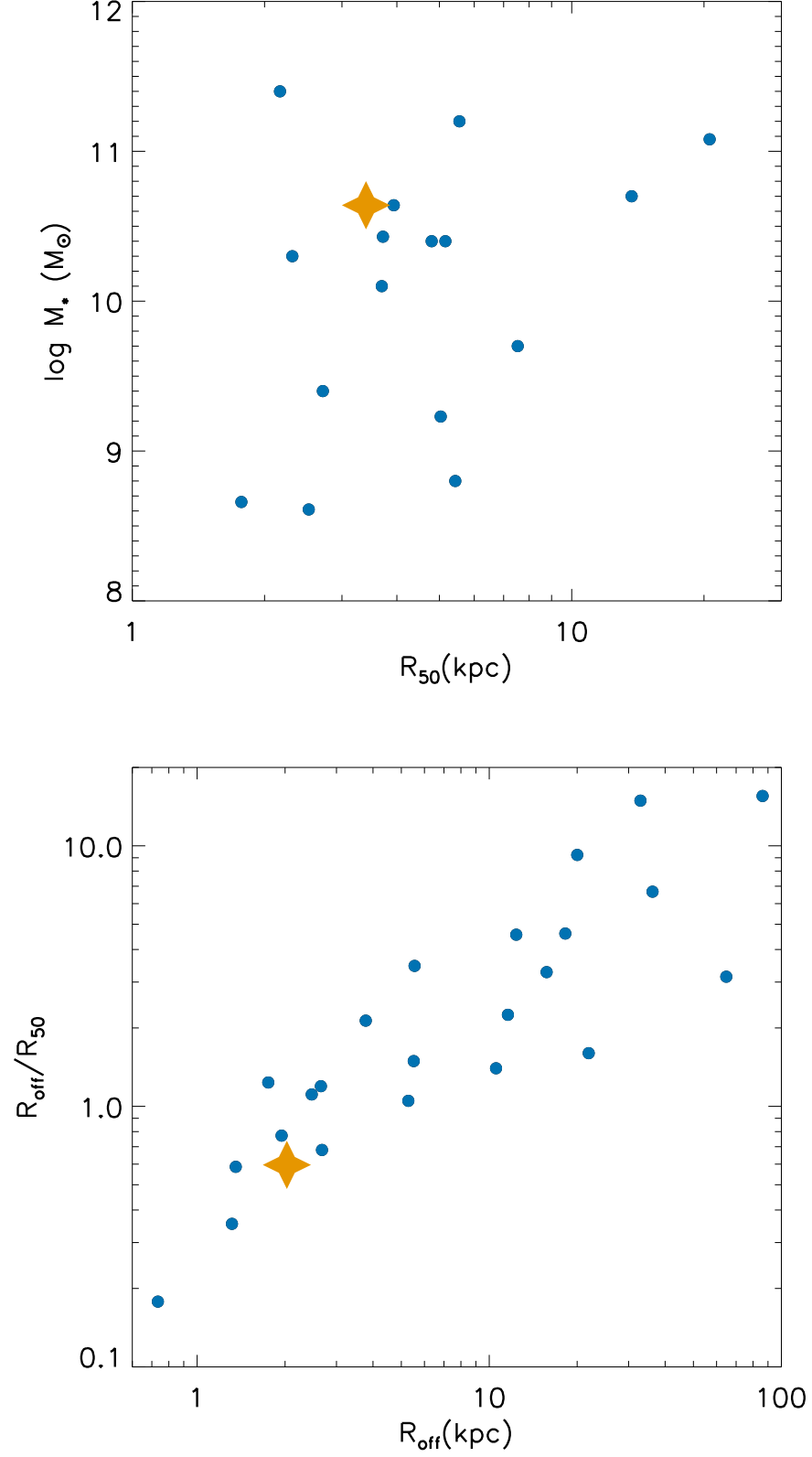


Figure S8: Top: A comparison of the half light radius R_{50} and stellar mass M_* [61] between GRB 170817A and other sGRBs. Bottom: A comparison of the physical offset R_{off} and normalized offset R_{off}/R_{50} between GRB 170817A and other sGRBs. The dots indicates sGRBs in [16]. The orange star presents NGC 4993, which falls well into the distributions of the sGRB host galaxy properties.

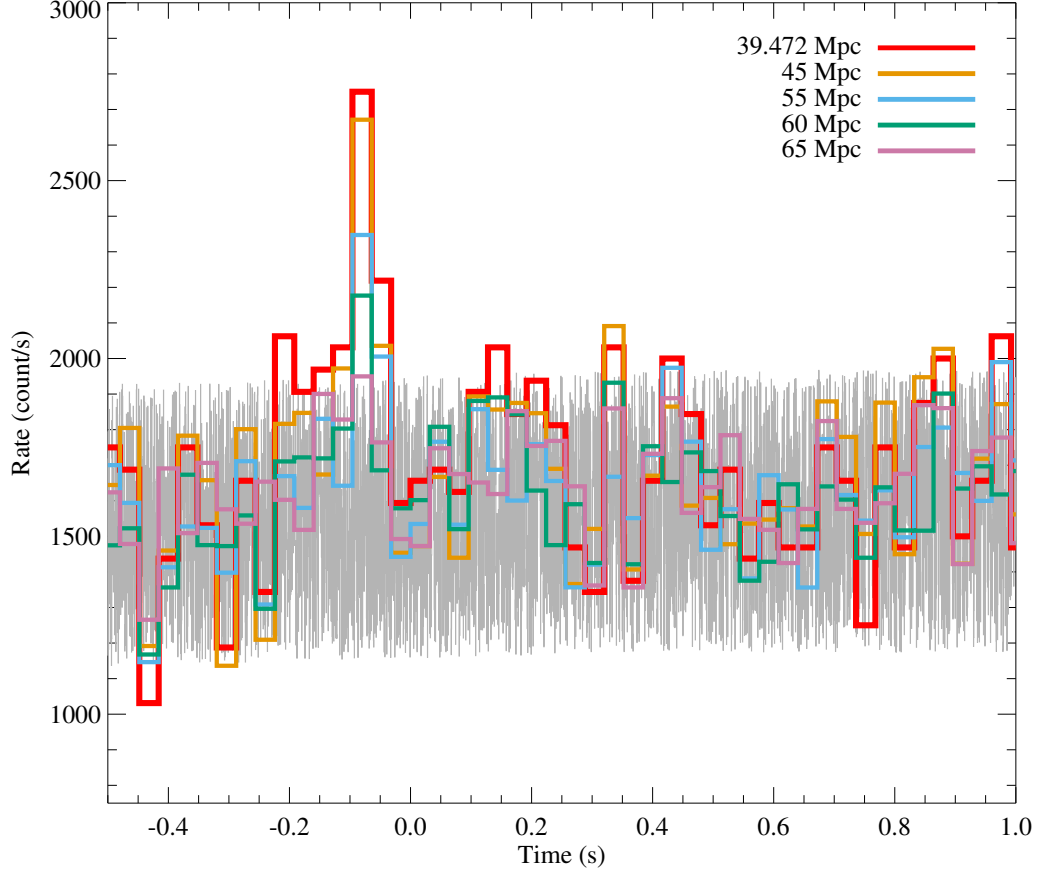


Figure S9: GRB 170817A and simulated bursts by placing it at different distances. A $1\text{-}\sigma$ Poisson noise was added for each simulation. At 65 Mpc, the burst becomes not detectable.

where,

$$\begin{cases} \dot{E}_{\nu\bar{\nu},\text{ign}} = 10^{(48.0+0.15a_{\bullet})} \left(\frac{m_{\bullet}}{3}\right)^{\log(\dot{m}/\dot{m}_{\text{ign}})-3.3} \text{erg s}^{-1}, \\ \alpha_{\nu\bar{\nu}} = 4.7, \quad \beta_{\nu\bar{\nu}} = 2.23, \quad \gamma_{\nu\bar{\nu}} = 0.3, \\ \dot{m}_{\text{ign}} = 0.07 - 0.063a_{\bullet}, \quad \dot{m}_{\text{trap}} = 6.0 - 4.0a_{\bullet}^3, \end{cases} \quad (10)$$

where \dot{m}_{ign} and \dot{m}_{trap} are the igniting and trapping accretion rates, respectively.

Adopting the same isotropic energy, one may need an accretion rate of $\dot{m} \sim 1.1 \times 10^{-2}$ for $m_{\bullet} = 3, a_{\bullet} = 0.7$, jet beaming factor $f_b \sim 0.01$ and efficiency of $\eta \sim 0.1$.

In either case, the required accretion rate is very low. In other words, a reasonably high accretion rate would likely over-predict the luminosity.

8. Intrinsically low-luminosity model - a millisecond pulsar engine

Neglecting gravitational wave spindown, the initial dipole spindown luminosity of a millisecond pulsar reads [45]

$$L_{\text{sd}} = 10^{47} \text{ erg s}^{-1} (B_{p,14}^2 P_{0,-3}^{-4} R_6^6), \quad (11)$$

where B_p is the surface magnetic field at the polar region, P_0 is the initial rotation period, and R is the radius of the pulsar, where the convention $Q = 10^n Q_n$ has been adopted in cgs units. Assuming $L_{\gamma} = \eta_{\gamma} L_{\text{sd}}$ where η_{γ} is an efficiency parameter, and assuming that the post-merger millisecond pulsar has a near-break-up spin period $P_0 \sim 1$ ms, in order to satisfy the luminosity constraint, the pulsar needs to have a magnetic field strength $B_p < 7.3 \times 10^{13} \text{ G } \eta_{\gamma}^{-1/2}$. Invoking gravitational wave spindown, which is likely for a post-merger remnant [46, 47], this constraint is less stringent. In any case, such a model predicts an underlying long-duration event, and the short duration event is just the brightest

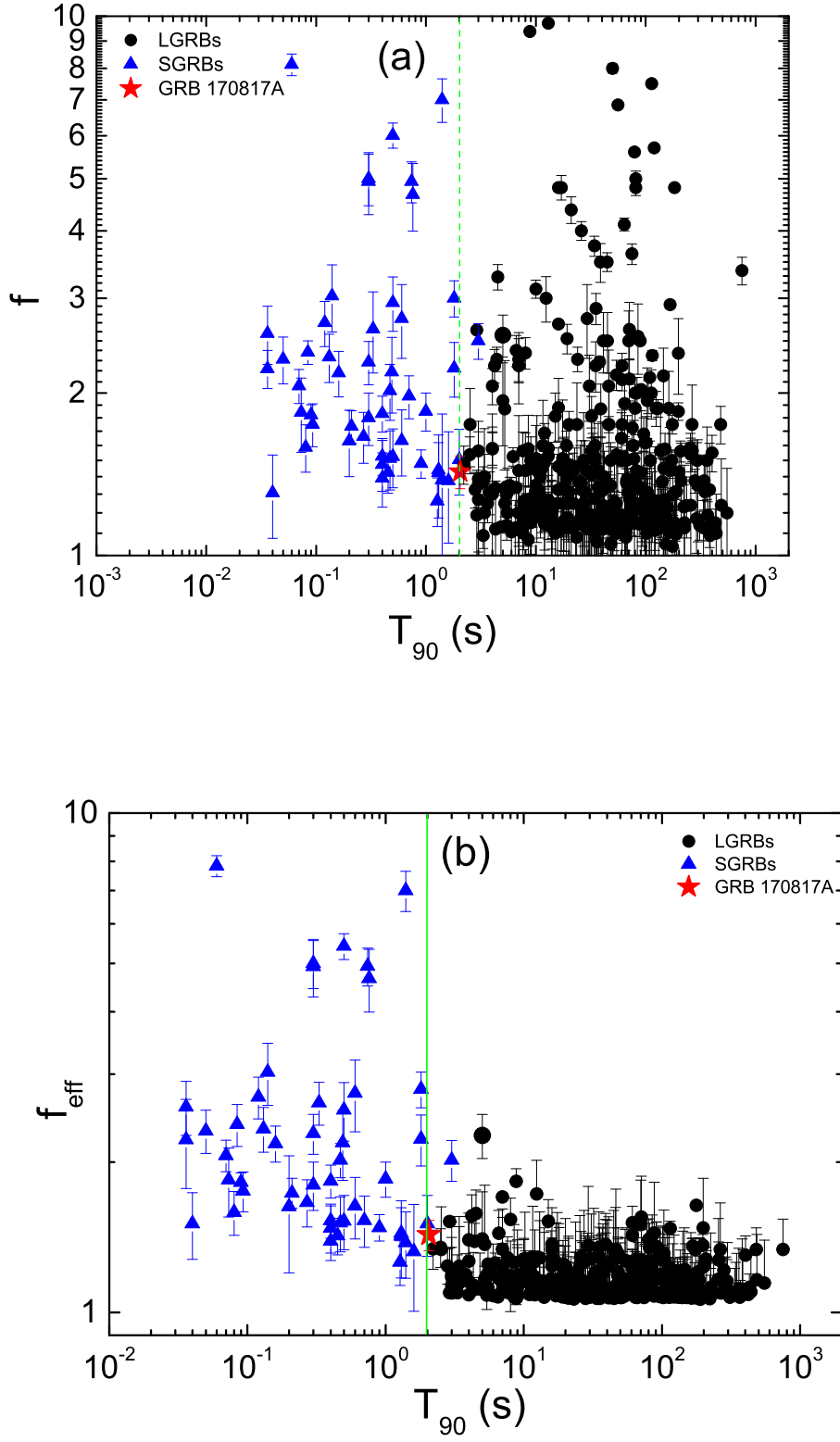


Figure S10: T_{90} vs. f and f_{eff} diagrams of both long and short GRBs taken from [33]. The red solid star is GRB 170817A, and the vertical line is $T_{90} = 2$ s.

tip of iceberg that sticks out from the background level. The search for this component leads to negative results. However, such a scenario cannot be ruled out due to the small amplitude factor f of the burst.

9. Delay time between the γ -ray event and the gravitational wave event

The merger time derived from the GW signal is $T_{GW}=12:41:04.4$ UTC on 17 August 2017[8] leads the GRB beginning time by $\Delta t \simeq 1.7$ s. This delay poses interesting constraints on the GRB emission models.

The BH accretion time scale is short. The fall-back time reads

$$t_{fb} \simeq 2 \left(\frac{R_{out}^3}{GM_{\bullet}} \right)^{1/2}, \quad (12)$$

where R_{out} is the outer edge of disk. Usually, we assume the accretion begins at $R_{out} \simeq 2R_T$, where R_T is the tidal disruption radius with $M_{\bullet}/R_T^3 \sim 4.2\rho_{NS}$. One thus finds,

$$t_{fb} \simeq 2 \left(\frac{2}{G\rho_{NS}} \right)^{1/2} \simeq 5 \times 10^{-4} s, \quad (13)$$

in which we adopt the typical density for neutron star (NS), i.e., $\rho_{NS} \sim 4 \times 10^{14} \text{ g cm}^{-3}$.

A more relevant timescale is the accretion timescale, which can be estimated as

$$\tau_{int} \simeq \frac{t_{fb}}{\alpha} \simeq 5 \times 10^{-3} \left(\frac{\alpha}{0.1} \right) s, \quad (14)$$

where α is the viscosity parameter. This time may be taken as the delay time between the formation of jet and the onset of accretion. One can see that this time scale is still much shorter than the observed delay.

A longer time scale comes from the propagation of the jet before releasing γ -rays. The delay time scale depends on the distance of the emission region from the central engine. In GRB models, both photosphere emission (which corresponds to a small radius $R_{ph} = L_w \sigma_T / (8\pi \Gamma^3 m_p c^3) \simeq (5.9 \times 10^{10} \text{ cm}) L_{w,47}^{1/2} \Gamma_1^{-3}$, where $L_w = 10^{47} \text{ erg s}^{-1}$, and $\Gamma = 10\Gamma_1$ is the Lorentz factor of the flow) and synchrotron radiation from an optically thin region ($R_{GRB} \gg R_{ph}$) have been invoked to interpret GRB emission.

Suppose that the GRB emission occurs at radius R_{GRB} with Lorentz factor Γ , the delay time from the launch of the jet to GRB emission is $t \sim R/2\Gamma^2 c$. The total delay time of the onset of the GRB with respect to the GW signal merger time would be [48]

$$\Delta t \sim (t + \tau_{int})(1 + z), \quad (15)$$

which is essentially defined by the jet propagation time t . Adopting $\Delta t = 1.7$ s from the data, the emission radius may be estimated as

$$R_{GRB} \sim 2\Gamma^2 ct = 1.0 \times 10^{15} \text{ cm} \left(\frac{\Gamma}{100} \right)^2 \left(\frac{\Delta t}{1.7 \text{ s}} \right) = 1.0 \times 10^{13} \text{ cm} \left(\frac{\Gamma}{10} \right)^2 \left(\frac{\Delta t}{1.7 \text{ s}} \right), \quad (16)$$

which is $\gg R_{ph}$. This suggests that emission is not from the photosphere radius. In order to suppress photosphere emission, one needs to invoke a Poynting flux dominated flow, [50] and synchrotron emission is generated at an optically thin region through certain magnetic dissipation mechanisms (e.g. [51]).

10. Predicted afterglow properties

The interaction between the jet and its ambient medium could generate a strong external shock, where particles are believed to be accelerated, giving rise to broad-band afterglow emission [52]. According to standard afterglow models, the lightcurve for a given observed frequency (e.g. optical frequency ν_{obs}) could be calculated as

$$F_{t,\nu_{obs}} = f(t, \nu_{obs}; z, p, n, \epsilon_e, \epsilon_B, E_k, \Gamma_0), \quad (17)$$

where E_k is the isotropic kinetic energy of the jet, Γ_0 is the initial Lorentz factor of the jet and n is the interstellar medium (ISM) particle number density. ϵ_e and ϵ_B are the electron and magnetic energy fraction parameters, and p is the electron spectral index.

Based on the total emission energy of the prompt emission and assume a factor of 20% for the γ -ray emission efficiency, the kinetic energy of the jet E_k can be estimated as $1.83 \times 10^{47} \text{ erg}$. For binary neutron star mergers, a low value for ambient medium density is usually expected, since they tend to have a large offset relative to the center of its host galaxy. Here we adopt the ambient medium density n as 10^{-3} cm^{-3} . For a structured jet viewed from a large

angle, the initial Lorentz factor may be low, so we adopt $\Gamma_0 = 20$. For other parameters, we adopt their commonly used values in GRB afterglow modeling, i.e., $\epsilon_e = 0.1$, and $p = 2.3$ [53, for a review]. The distribution of the ϵ_B value is wide, from $\epsilon_B = 0.01$ to $\epsilon_B < 10^{-5}$ [54–58].

We use $\epsilon_B = 0.01$ to calculate the most optimistic case of afterglow emission. The peak flux of the X-ray light curve emerges around 2000s, at the level of 10^{-14} erg/cm²/s. Around 1 day, the X-ray flux will decay to the level of 10^{-15} erg/cm²/s, under the detection limit of Swift/XRT. This is consistent with the non-detection result by the *Swift* team [59]. For optical band, the peak of the light curve appears around 2000 s, and the peak flux is 1 μJy (AB magnitude is 24). Around 1 day, the optical flux decays to the level of 0.01 μJy (AB magnitude is 28). This is much lower than the observed flux. This suggests that the optical transient detected by us and by multiple groups originates from the emission of a kilonova or mergernova [28–30, 60].

11. Search for GRB 170817A-like events

Since it is possible that there are other GRB 170817A-like events in the GBM faint sGRB sample, we attempted to search for these events using the galaxy data. We choose all the faint bursts listed in Supplementary Figure S7, and look for NGC 4993-like galaxy (with luminosity 3.6×10^{43} erg s⁻¹) below 80 Mpc within the error boxes of the sGRBs. Supplementary Figure S11 shows the galaxies (red dots) with luminosity $> 10^{43}$ erg s⁻¹ (left) and $> 3 \times 10^{43}$ erg s⁻¹ (right) compared with sGRB error circles. It is clearly seen that the error circles are too large and typically enclose many galaxies. So identifying GRB 170817A-like events is difficult without gravitational wave detections.

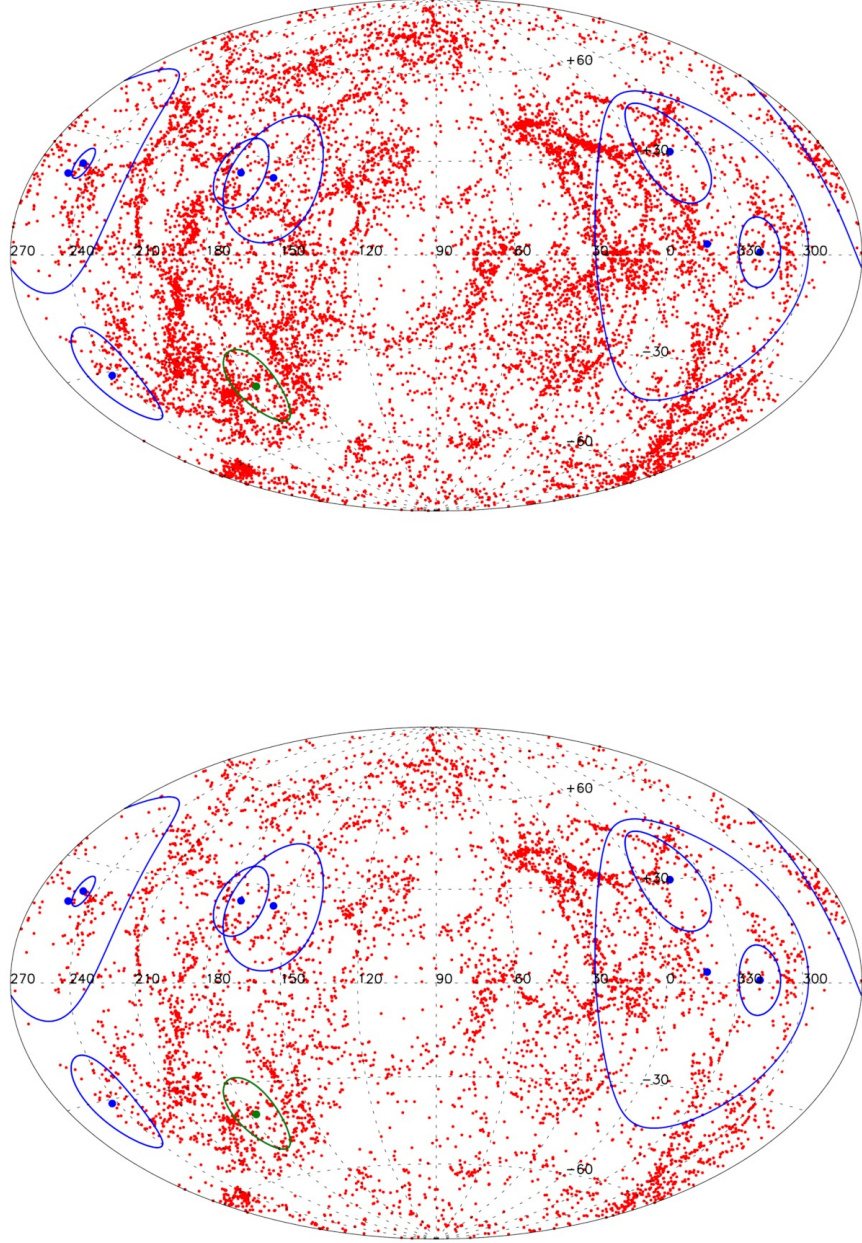


Figure S11: The position error circles of GRB 170817A-like sGRBs in Figure S7 compared with the sky map of galaxies below 80 Mpc with two different luminosity threshold: $> 10^{43} \text{ erg s}^{-1}$ (top) and $> 3 \times 10^{43} \text{ erg s}^{-1}$ (bottom). The green color indicates GRB 170817A.

-
32. Kass, R. E. & Wasserman, L., A reference Bayesian test for nested hypotheses and its relationship to the Schwarz criterion., *J. Am. Stat. Assoc.* **90**, 928-934 (1995)
 33. Lü, H.-J., Zhang, B., Liang, E.-W., Zhang, B.-B., & Sakamoto, T., The ‘amplitude’ parameter of gamma-ray bursts and its implications for GRB classification, *Mon. Not. R. Astron. Soc.* **442**, 1922-1929, (2014)
 34. Zhang, B., et al., Discerning the Physical Origins of Cosmological Gamma-ray Bursts Based on Multiple Observational Criteria: The Cases of $z = 6.7$ GRB 080913, $z = 8.2$ GRB 090423, and Some Short/Hard GRBs, *Astrophys. J.* **703**, 1696-1724, (2009)
 35. Blandford, R. D., & Znajek, R. L., Electromagnetic extraction of energy from Kerr black holes, *Mon. Not. R. Astron. Soc.* **179**, 433-456 (1977)
 36. Lee, H. K., Wijers, R. A. M. J., & Brown, G. E., The Blandford-Znajek process as a central engine for a gamma-ray burst, *Phys. Rep.* **325**, 83-114 (2000)
 37. Tchekhovskoy, A., Narayan, R., & McKinney, J. C., Efficient generation of jets from magnetically arrested accretion on a rapidly spinning black hole, *Mon. Not. R. Astron. Soc.* **418**, L79-L83 (2011)
 38. Lei, W.-H., Zhang, B., & Liang, E.-W., Hyperaccreting Black Hole as Gamma-Ray Burst Central Engine. I. Baryon Loading in Gamma-Ray Burst Jets, *Astrophys. J.* **765**, 125 (2013)
 39. Popham, R., Woosley, S. E., & Fryer, C., Hyperaccreting Black Hole and Gamma-Ray Bursts, *Astrophys. J.* **518**, 356-374 (1999)
 40. Chen, W. X., & Beloborodov, A. M., Neutrino-cooled Accretion Disks around Spinning Black Holes, *Astrophys. J.* **657**, 383-399 (2007)
 41. Januik, A., Yuan, Y., Perna, R., & Di Matteo, T., Instabilities in the Time-Dependent Neutrino Disk in Gamma-Ray Bursts, *Astrophys. J.* **664**, 1011-1025 (2007)
 42. Liu, T., Gu, W. M., & Zhang, B., Neutrino-dominated accretion flows as the central engine of gamma-ray bursts, 2017, *New Astron. Rev.* in press, [arXiv:1705.05516](https://arxiv.org/abs/1705.05516) (2017)
 43. Zalamea, I., & Beloborodov A. M., Neutrino heating near hyper-accreting black holes, *Mon. Not. R. Astron. Soc.* **410**, 2302-2308 (2011)
 44. Lei, W.-H., Zhang, B., Wu, X.-F., & Liang, E.-W., Hyperaccreting Black Hole as Gamma-Ray Burst Central Engine. II. Temporal evolution of central engine parameters during Prompt and Afterglow Phases, *ArXiv e-prints*, [arXiv:1708.05043](https://arxiv.org/abs/1708.05043) (2017)
 45. Zhang, B. and Mészáros, P., Gamma-Ray Burst Afterglow with Continuous Energy Injection: Signature of a Highly Magnetized Millisecond Pulsar, *Astrophys. J.* **552**, L35-L38 (2001).
 46. Gao, H., Zhang, B., & Lü, H.-J., Constraints on binary neutron star merger product from short GRB observations, *Phys. Rev. D* **93**, 044065 (2016)
 47. Piro, A.L., Giacomazzo, B., and Perna, R., The Fate of Neutron Star Binary Mergers, *Astrophys. J.* **844**, L19 (2017).
 48. Zhang, B.: 2016, Mergers of Charged Black Holes: Gravitational-wave Events, Short Gamma-Ray Bursts, and Fast Radio Bursts, *Astrophys. J.* **827**, L31 (2016)
 49. Mészáros, P., & Rees, M. J., Steep Slopes and Preferred Breaks in Gamma-Ray Burst Spectra: The Role of Photospheres and Comptonization, *Astrophys. J.* **530**, 292-298 (2000)
 50. Zhang, B., & Pe’er, A., Evidence of an Initially Magnetically Dominated Outflow in GRB 080916C, *Astrophys. J.* **700**, L65-L68 (2009)
 51. Zhang, B., & Yan, H., The Internal-collision-induced Magnetic Reconnection and Turbulence (ICMART) Model of Gamma-ray Bursts, *Astrophys. J.* **726**, 90 (2011)
 52. Gao, H., Lei, W.-H., Zou, Y.-C., Wu, X.-F., & Zhang, B., A complete reference of the analytical synchrotron external shock models of gamma-ray bursts, *New Astro. Rev.* **57**, 141-190 (2013)
 53. Kumar, P., & Zhang, B., The physics of gamma-ray bursts & relativistic jets, *Phys. Rep.* **561**, 1-109 (2015)
 54. Santana, R., Barniol Duran, R., & Kumar, P., Magnetic Fields in Relativistic Collisionless Shocks, *Astrophys. J.* **785**, 29 (2014)
 55. Wang, X.-G., et al., How Bad or Good Are the External Forward Shock Afterglow Models of Gamma-Ray Bursts?, *Astrophys. J. Suppl. S.* **219**, 9 (2015)
 56. Beniamini, P., Nava, L., Duran, R. B., & Piran, T., Energies of GRB blast waves and prompt efficiencies as implied by modelling of X-ray and GeV afterglows, *Mon. Not. R. Astron. Soc.* **454**, 1073-1085 (2015)
 57. Zhang, B.-B., van Eerten, H., Burrows, D. N., Ryan, G. S., Evans, P. A., Racusin, J. L., Troja, E., & MacFadyen, A., An Analysis of Chandra Deep Follow-up Gamma-Ray Bursts: Implications for Off-axis Jets, *Astrophys. J.* **806**, 15 (2015)
 58. Ryan, G., van Eerten, H., MacFadyen, A., & Zhang, B.-B., Gamma-Ray Bursts are Observed Off-axis, *Astrophys. J.* **799**, 3 (2015)
 59. Evans, P. A. et al., *Swift* and *NuSTAR* observations of GW170817: detection of a blue kilonova, *Science*, doi:10.1126/science.aap9580 (2017)
 60. Kulkarni, S. R., Modeling Supernova-like Explosions Associated with Gamma-ray Bursts with Short Durations, *ArXiv Astrophysics e-prints*, [arXiv:astro-ph/0510256](https://arxiv.org/abs/astro-ph/0510256), (2005)
 61. Ogando, R.L.C., et al., Line Strengths of Early-Type Galaxies, *Astron. J.* **135**, 2424-2445 (2008).